Construction of a plan library for high risk prostate cancer patients in proton therapy

Abal Bonny

Master Thesis in Medical Physics and Technology

Department of Physics and Technology
University of Bergen, Norway

June 8, 2017

Declaration

I, Bonny Abal, declare that this thesis is my work and has never been submitted to any University before for an award of any degree and that the thesis was done under the supervision of Associate Prof. II Sara Thönqvist and Associate Prof. II Liv Bolstad Hysing.

Dedication

This piece of work is dedicated to my wife Dorine, mummy Esther and mummy Perpetua.

Acknowledgement

My sincere thanks go to the Almighty God for having granted me this opportunity to reach this stage with good health and sound mind. It has not been easy but You gave me the courage and strength. Secondly, alot of thanks go to my thesis supervisors: Associate Prof. II Sara Thönqvist and Associate Prof. II Liv Bolstad Hysing both of the Department of Physics and Technology of University of Bergen and Medical Physics Department of Haukeland University Hospital. The doors to your offices were always open whenever I ran into a trouble spot or had a question about my research and writing. You consistently allowed this paper to be my own work, but steered me in the right direction whenever you thought I needed it.

I would also like to thank the following people who were involved in the validation survey for this research project: Grete May Engeseth of the Department of Oncology and Medical Physics of Haukeland University Hospital, and Kristian Ytre-Hauge, a Researcher at the Department of Physics and Technology at the University of Bergen. Without your passionate participation and input, the validation of the results could not have been successfully conducted.

I would also like to acknowledge Prof. Dieter Röhrich of the Department of Physics and Technology for the rich knowledge you imparted in Radiation Physics and I am gratefully indebted to your parental guidance whenever I needed.

Finally, I must express my very profound gratitude to my parents and to my dear wife, Dorine for providing me with unfailing support and continuous encouragement throughout my years of study and through the process of researching and writing this thesis. This accomplishment would not have been possible without you. Thank you.

Contents

List of Figures

List of Tables

List of Acronyms

APT	Adaptive Proton Therapy
ART	Adaptive Radiation Therapy
AS	Active Surveillance
CT	Computed Tomography
CTV	Clinical Target Volume
EAU	Eauropean Association of Urology
EBRT	External-Beam Radiation Therapy
EUD	Equivalent Uniform Dose
HDR-BT	High Dose Rate Bracytherapy
HFRT	Hypofractionated Radiotherapy
ICRU	International Commission on Radiation Units and Measurements
IGRT	Image-Guided Radiation Therapy
IMPT	Intensity Modulated Proton Therapy
IMRT	Intensity Modulated Radiotherapy or Radiation Therapy
LBL	Lawrence Berkeley Laboratory
LDR-BT	Low Dose Rate Bracytherapy
LQE	Linear Quadratic Equation
LINAC	Linear Accelerator
MRI	Magnetic Resonance Imaging
OAR	Organs At Risk
PBS	Pencil Beam Scanning
PCa	Prostate Cancer
PET	Positron Emission Tomography
PSA	Prostate-specific Antigen
PTCOG	The Proton Therapy Cooperative Group
RBE	Relative Bioligical Effectiveness
RP	Radical Prostatectomy
RT	Radiotherapy
SBRT	Stereotactic Body Radiotherapy
SOBP	Spread-Out Bragg Peak
SPECT	Single-Photon Emission Computed Tomography
VMAT	Volumetric Modulated Arc Therapy
3D-CRT	Three-Dimensional Conformal Radiation Therapy

Abstract

High-risk prostate cancer patients can receive treatment of both the pelvic lymph nodes and seminal vesicles, in addition to the prostate based on an estimated risk of lymph node spread. Due to the large volume being irradiated, these patients could be an attractive sub-group for proton therapy. The primary advantages of proton therapy is that it causes less damage to healthy surrounding tissues than photon therapy dose and improves the conformity of the dose to the target. In regard to normal tissue, proton therapy therefore provides great potential in sparing normal tissue and reduce unwanted side-effects, but if the reduced dose leads to a reduction in toxicity has yet to be documented. The involvement of three target structures and the independent motion of these regions make delivery of the treatment with protons challenging.

Adapting the treatment to the target motion of the patients during the course of treatment could be a solution [Yan D. et al., 2010]. A resource effective method since online re-optimisation is not yet feasible when delivering the treatment, can be to construct a plan library with different positions of the prostate in regards to the lymph nodes, which previously has been applied for radiotherapy [Xia P. et al., 2010]. This Master project will investigate if this strategy can be extended to proton therapy. The plan library was generated based on an initial analysis of prostate motion relative to bony anatomy in 18 patients (Study A).

The output from study A was then used as an input for study B. In study B, we created a pool of three plans in addition to a standard plan for each patient basing on a planning computed tomography (pCT) and optimized each plan to accommodate a presumed prostate position. The three plans were for the prostate in three different locations with respect to the pelvic lymph nodes, including the original prostate contour and two contours shifted +/-5mm in an anterior-posterior (AP) direction and +/-4.6mm in cranial-caudal (CC) direction simultaneously. Prostate only (CTV67.5), prostate together with seminal vesicles (CTV60) and lymph nodes (CTV50) were the clinical target volumes (CTVs); and planning target volumes (PTVs) were created around the CTVs with an isotropic margin of 5mm. We compared this strategy to the standard treatment strategy with respect to the doses on the targets, rectum and bladder. The standard plan had a larger margin compared to the plan library with 5mm margin for PTV50 around CTV50, 3mm margin in the left-right and 10mm margins in both the cranial-caudal and anterior-posterior directions for PTV67.5 around CTV67.5; and 5mm margin in left-right and 10mm in both cranial-caudal and anterior-posterior directions for PTV60 around CTV60. The prostate margin was determined uisng the Van Herk's formula as part of the motion analysis in study A. The results showed similar doses to the targets as in the standard treatment approach but with reduced gEUD to the rectum (k=12) and bladder (k=8). Similar doses were also obtained for both small (k=4) and large (k=4) bowels in the two strategies. The plan library approach for treatment of high-risk prostate cancer patients therefore proved feasible.

Chapter 1: Introduction

1.1 High Risk Prostate Cancer and its treatment

There is no exact definition of high risk prostate cancer. Cancer incidences and survival generally for prostate and especially high-risk, clinically localised prostate cancer was defined as any combination of the following factors: a prostate-specific antigen (PSA) score >20 ng/ml, a Gleason score of 8 - 10, or clinical stage T2c or greater [D'Amico et al., 2002]. More recently, the National Comprehensive Cancer Network and European Association of Urology (EAU) modified this definition to include any combination of a clinical T3, a PSA score >20 ng/ml, or a Gleason score of 8 - 10 [Albert J. et al., 2014]. Independent of the definition used, the optimal treatment for these men remains unknown, but the common treatments for prostate cancer in general include surgery, radiation therapy (RT), or primary androgen-deprivation therapy. External beam radiation therapy (EBRT) is the most widely used type of radiation therapy, and it most often uses photon beams. The radiation comes from a machine outside the body and is focused on the cancer, by irradiating the patients from various angles. This type of radiation is most often given by machines called linear accelerators (LINACS). External beam radiation can be used to treat large areas of the body. It can also be used to treat more than one area, such as the main tumor and the nearby lymph nodes.

Trials and experience from larger treatment centres show that when RT is adequately administered, it can achieve cure rates that is comparable to surgical treatment for localised prostate cancer [Chuba et al., 2001; Kupelian et al., 2002; Potosky et al., 2000]. Furthermore, studies on quality of life and side effects indicate that, despite a wide range of complications, the overall impact of these treatment modalities on the well being of the patients is comparable [Kupelian et al., 2002; Madalinska et al., 2001; Wei et al., 2002]. The use of whole pelvic radiotherapy (WPRT) is controversial in patients with locally advanced prostate adenocarcinoma [Ayal A. A. et al., 2009]. Theoretically, WPRT, in comaprison to prostate-only RT (PORT), improves outcome in patients with advanced or aggressive PCa by sterilizing the locoregional lymph nodes on assumption that the lymph nodes may harbour occult disease before more distant sites [Ayal A. A. et al., 2009, Lisa K. Morikawa et al. 2011]. WPRT is prescribed since it is difficult to detect lymph node metastases clinically as prostate cancer has the potential to spread to numerous lymph node groups. Besides, there is inaccuracy in determination of lymph node involvement of patients with prostate cancer due to many reasons such as poor sensitivity of CT, magnetic resonance imaging (MRI), and positron emission tomography (PET). If patients in the PORT and WPRT cohorts were to have equivalent intrinsic tumor characteristics, it is possible that the WPRT arm would have displayed improved biochemical-disease free survival compared with the PORT arm. With regard to the adverse effects, acute toxicity appeared to be greater in the WPRT patients, but no difference was found in the incidence of late toxicity [Ayal A. A. et al., 2009]. However, patients undergoing WPRT displayed an increased incidence of acute gastrointestinal toxicity relative to those treated with PORT and a greater percentage of WPRT patients experienced acute genitourinary toxicity, although this difference was not statistically significant. No difference in late genitourinary or gastrointestinal toxicity was seen between the two cohorts [Ayal A. A. et al., 2009].

At Haukeland University Hospital, high-risk prostate cancer patients get treatment of the prostate, lymph nodes and seminal vesicles. A high dose of 67.5 Gy is delivered to the prostate only, a dose of 60 Gy to both the prostate and seminal vesicles while a low dose of 50 Gy is delivered to the lymph nodes only. The three dose levels are delivered as a simultaneous integrated boost (SIB) delivered in 25 fractions over a time interval of five weeks.

1.2 History of Radiotherapy

Radiotherapy refers to the treatment of disease (cancer) with radiation, especially by selective irradiation with x-rays or other ionizing radiation such as gamma rays and charged particles. RT delivery can be done as EBRT, which may be conventionally fractionated RT(CFRT) with intensity modulated radiation therapy (IMRT) or protons, hypofractionated RT (HFRT) with IMRT or protons, or delivered as stereotactic body RT (SBRT); or as brachytherapy (BT), which can be either high dose rate BT (HDR-BT) or low dose rate BT (LDR-BT). RT dates back to the discovery of x-rays.

Wilhelm Rontgen announced the discovery of X-rays on November 30^{th}, 1895. At the end of January 1896, approximately 60 days after Rontgen's announcement, Emil Grubbe, a second-year medical student treated the first two patients with X-rays. The first was breast cancer and the other, skin lesions due to Tuberculosis and hence the birth of radiation therapy [Lederman M.,

1981]. Since then, radiation therapy has been constantly developing for the last 120 years, but the aim has always been the same, to deliver as close as possible to 100% of the prescribed dose to the target volume, while at the same time spare as much of the healthy tissue as possible. The advancements in that line since 1895 have been tremendous.

In the beginning, treatments were available for only superficial tumors and melanomas, due to the relatively low photon energies that were achievable. Years later, both supervoltage X-ray tubes and LINACS were developed, which allowed for treatment of more deep-seated tumors. As early as 1906, different patterns of radiosensitivity were demonstrated, and in 1934 radiation dose deliverance using fractionation, as opposed to delivering the entire dose at the same time, was proposed [Thariat J. et al., 2012]. This technique together with many more have led to better cure rates for cancer and less damage to healthy tissue [Thariat J. et al., 2012]. In 1953, the first LINAC for photon therapy was installed in London. This was only a few years after Robert Wilson's emphasis on the therapeutic advantage of using protons in radiation therapy in his article Radiological Use of Fast Protons [R. R. Wilson, 1946]. He also proposed the use of heavier ions. As stated, the first patient was treated with protons as early as 1954, while treatments using helium and neon ions were first done in 1957 and 1975, respectively [Amaldi U. and Kraft G., 2005]. After the 1960s, the definitions of target volumes and organs at risk were made by the International Commission on Radiation Units and Measurements (ICRU) and also treatment planning systems arrived, allowing more accurate treatment planning [Thariat J. et al., 2012].

Another break through by Godfrey Hounsfield by developing the CT scanner in 1971 paved way to radiation planning shifting from two to three dimensions later when more than one slice was acquired with CT. Consequently, CT-based simulations and dose planning were introduced, and computer driven multileaf collimators (MLC) conforming the radiation field, were developed in the 1990s. In the early 2000s, intensity-modulated radiation therapy (IMRT), followed by volumetric modulated arc therapy (VMAT) and image guided radiation therapy (IGRT) had a significant effect on the success of radiation therapy. The many delivery techniques and methods developed in the last century have made it possible to personalize the radiation therapy techniques based on different types of patients, tumor extents and locations. However, the spatial dose distribution from photons must unfortunately follow the laws of physics, meaning that the conformity of high dose volumes with photons is actually as good as with protons, but at the proce of a larger "dose bath".

1.3 Proton Therapy

Proton therapy has been used since 1954. Cyclotron facilities that produced proton beams previously existed for physics research, but in 1946, Robert Wilson first proposed they be used for the treatment of cancer.This relates to the importance of highly localized deposition of energy as a way of increasing the dose to the tumour, while minimizing the dose to normal tissues [Pugh T.J. and Lee A.K., 2014]. Two years later, researchers at the Lawrence Berkeley Laboratory conducted extensive studies on protons and confirmed the predictions made by Wilson. The first treatments on humans consisted of radiation to destroy the pituitary gland in patients with hormone-sensitive metastatic breast cancer [Shinohara E., 2016]. This treatment successfully stopped the pituitary from making the hormones that stimulated the cancer cells to grow. In the 1950's, the treatments were effectively duplicated on patients at a facility in Uppsala, Sweden [Shinohara E., 2016].

This led to the Harvard Cyclotron Facility using protons for medical treatments. They began treatment of the pituitary gland and developed specialized techniques for treating other conditions such as arteriovenous malformations (AVM) [Shinohara E., 2016]. During the 1960's, these facilities worked to expand proton treatments to include choroidal melanomas, chondrosarcomas, chordomas, and various cancers located in the brain. However, this early work was limited due to the inability to perform 3-D imaging and the reliance on treatment in facilities primarily dedicated to physics research [Shinohara E., 2016].
In the 1980's, design and construction began on the first dedicated clinical proton facility at Loma Linda University Medical Center in California, which has treated over 18,000 patients with proton therapy.

Over 130,000 patients have now been treated with proton therapy worldwide [Shinohara E., 2016]. There are 19 facilities operating in the U.S. with several facilities currently under construction or in the planning stages. Many experts argue that without clinical trials, the therapy is not proven to be superior to x-ray therapy [Shinohara E., 2016]. Some centers are making clinical trials a priority to help determine which cancers are best treated by protons.

Just as X-rays (also known as photons) are used to treat both benign and malignant tumors, proton beams can be used to irradiate tumors in a similar way, which is referred to as proton

therapy. There is no significant difference in the biological effects of protons versus photons (x-rays). Protons deliver a dose of radiation much more precisely than photons. After they enter the body, protons release most of their energy within a defined depth and, unlike photons, deliver only a minimal dose beyond this range. Therefore, the dose of radiation may, because of less integrated dose (i.e. at entrance and exit), conform much tighter to the tumor and there may be less damage to healthy tissue. As a result, the treating physician (a radiation oncologist) can potentially prescribe an even greater dose to the tumor without increasing risk of unwanted side effects. Proton beam therapy uses special machines, a cyclotron and synchrotron being the most common, to generate and accelerate protons to speeds up to 60 percent the speed of light and energies of up to 250MeV. A cyclotron is a device made of a cylindrical or spherical chamber and uses a high-frequency alternating voltage or rapidly varying electric field to generate and accelerate protons to high speeds which are normally used in used in production of radioactive isotopes. Where as a synchrotron is made of a torus shaped tube,and uses varying electric and magnetic fields to generate and accelerate protons to high speeds and they are used in most of the large-scale facilities such as in carbon ion therapy. These high-energy protons are steered by magnets toward the treatment room, and then to the specific part of the body being treated. About 154,203 patients have been treated with particle therapy from 1954-2015 out of which 131,240 were treated with protons [Martin J., 2015]. In first generation proton machines, additional pieces of equipment such as a degrader, a modulator wheel, a range shifter wheel are needed to modify the range of the protons and the shape of the beam [Shinohara E., 2016]. Newer facilities make similar adjustments by fine tuning the energy of the beam and the magnetic fields which guide their path ("pencil beam scanning" or "scanning beam"). A beam degrader can be used to change the energy of the proton beam. This energy selection system degrades the initial beam produced by the cyclotron to produce several different lower energies [Shinohara E., 2016]. This allows the beam energy to be modulated such that a variety of depths within the tissue can be treated. These modifications guide the proton beam to precise locations in the body where they deliver the energy needed to inactivate tumor cells.

Chapter 2: Theoretical background of (radio and) particle therapy

Photon therapy and proton therapy are both radiotherapy techniques but the former uses photons to irradiate diseased tissues while the latter uses beams of energetic protons, which have very different physical properties. Before reaching the tumor, both radiation types pass/penetrate through the patients skin and surrounding tissues (entrance dose). To deliver a high dose to the target, multiple fields are usually used as shown in the Figure 1 below.

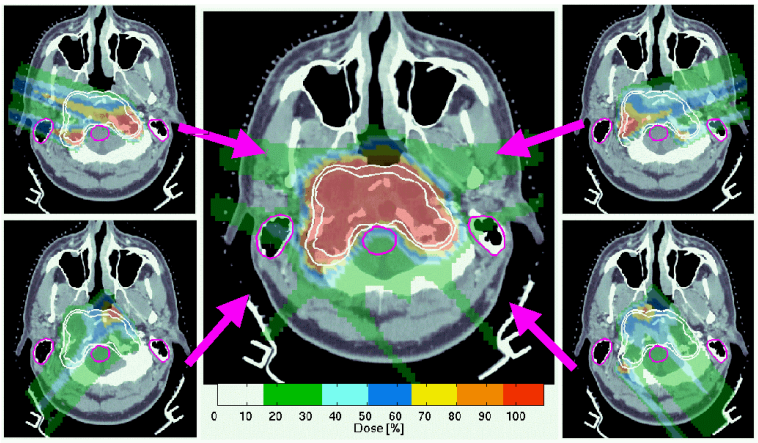

Figure 1: Illustration of multiple fields in radiotherapy [Alex T., Massachusetts General Hospital, 1994].

In this chapter, physical interactions of photons and protons will be discussed as these forms the basis of how treatment is performed. Biological effects and relative biological effectiveness (RBE) will also be presented to understand how radiations interact with the tissues. Last but not least, techniques of photon therapy and proton therapy will be presented for the understanding of how these modalities are used.

2.1 Physical interaction of photons

The photon, with no mass and no charge, is highly penetrating and delivers a dose throughout any volume of tissue irradiated. However, most of the radiation is delivered only 0.5 to 3 cm from the patients skin, depending on the energy it was initially given. It then gradually attenuates until it reaches the target ,and as photons are not all stopped by human tissue, they leave the patient's body and continue to emit radiation (exit dose).
High-energy photons is the most common form of radiation used in RT today [Michael J.G. et al., 2005]. Photons are either released from the nucleus of a radioactive atom and are known as gamma rays or they are created electronically, such as in a clinical LINAC, and they are known as x-rays. Photon absorption in human tissue is determined by the energy of the radiation, as well as the atomic structure of the tissue in question. Since the energies of the photons coming from LINAC has a distribution of energies, the voltage of the LINAC is usually used, i.e. MV, to describe the photon energy in clinical practice.

2.1.1 Photon-tissue interactions

Three interactions describe photon absorption in tissue: the photoelectric effect, Compton effect, and pair production;

(a) Photoelectric effect
In this process, an incoming photon undergoes a collision with a tightly bound electron. The photon transfers practically all of its energy to the electron and ceases to exist. The electron departs with most of the energy from the photon and begins to ionize surrounding molecules. This interaction depends on the energy of the incoming photon, as well as the atomic number of the tissue; the lower the energy and the higher the atomic number,the more likely that a photoelectric effect will take place [Michael J.G. et al., 2005].
An example of this interaction in practice can be seen on a diagnostic x-ray film. Since the atomic

number of bone (13.8) is 60% higher than that of soft tissue (7.4), bone is seen with much more contrast and detail than is soft tissue. The energy range in which the photoelectric effect predominates in tissue is about 10-25 keV [Michael J.G. et al., 2005].

(b) Compton effect
Compton effect is the dominant photon-tissue interaction for the treatment of cancer with photons. In this case, a photon collides with a "free electron," that is, one which is not tightly bound to the atom. Unlike the photoelectric effect, in the Compton interaction both the photon and electron are scattered. The Compton effect (also called Compton scattering) is when a high-energy photon collides with a target,following release of a loosely bound electron from the outer shell of the atom or molecule [Jared H., 2005].

The photon can then continue to undergo additional interactions, albeit with a lower energy. The electron begins to ionize with the energy given to it by the photon. The probability of a Compton interaction is inversely proportional to the energy of the incoming photon and is independent of the atomic number of the material. As a result, when an image of tissue is acquired using photons in the energy range in which the Compton effect dominates ($\approx$ 25 keV - 25 MeV), bone and soft tissue interfaces are barely distinguishable. The Compton effect is the most common interaction occurring clinically, as most radiation treatments are performed at energy levels of about 6 - 20 MeV.

(c) Pair production
In this process, a photon interacts with the nucleus of an atom, not an orbital electron. The photon gives up its energy to the nucleus and, in the process, creates a pair of positively and negatively charged electrons. In order for pair production to occur, the incoming energy of the interaction must be above a threshold (1.02MeV) in order to create the pair- atleast the total rest mass energy of the two particles and that the situation allows both energy and momentum to be conserved. The positive electron (positron) ionizes until it combines with a free electron and annihilates into two photons that scatter in opposite directions [Michael J.G. et al., 2005]. The probability of pair production is proportional to the logarithm of the energy of the incoming photon and is dependent on the atomic number of the material. The energy range in which pair production dominates is $\geq$ 25 MeV. However, this interaction does occur to some extent in routine radiation treatment with high-energy photon beams.
The graph below (Figure 2) shows the region where the different interactions dominate with respect to the relative importance of the three main interaction mechanisms depending on the energy of the incident photon and the nature of the absorbing material.

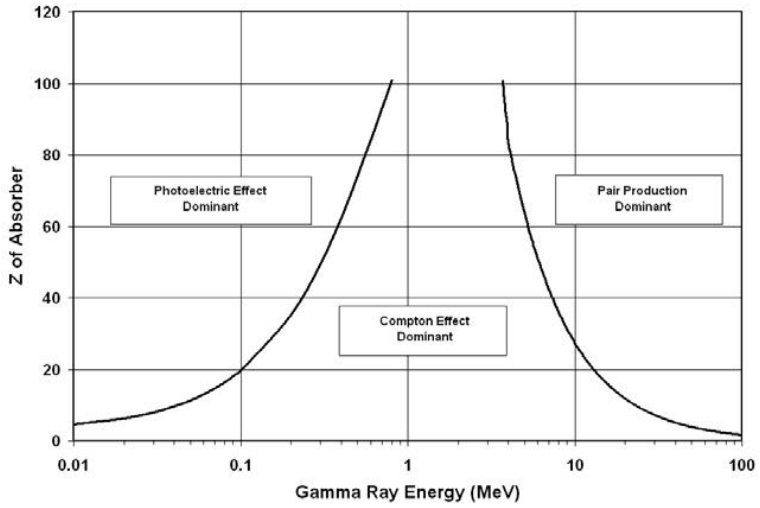

Figure 2: Graph of atomic mass, Z versus energy illustrating the dominance of the three different interaction mechanisms of photons [Dr. James E. Parks, 2004].

2.2 Physical interaction of protons

The proton is a charged particle that gradually looses its velocity as it interacts with human tissue. Proton has high energy when it enters the patient's body and only a small radiation dose is inadvertently deposited in normal tissues before the radiation reaches the tumour. The absorbed

dose increases gradually with greater depth and lower speed, suddenly rising to a peak when the proton is ultimately stopped. This peak is termed the Bragg peak (Figure 3).

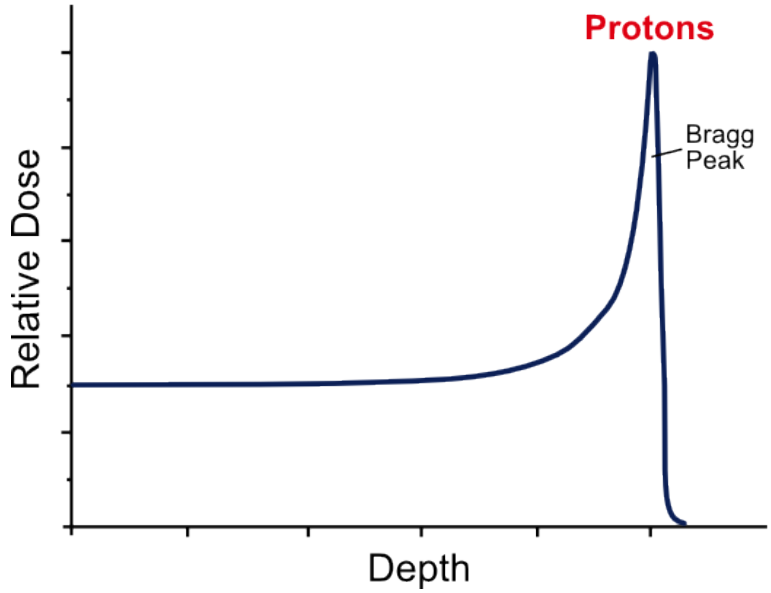

Figure 3: Graph of relative dose against depth illustrating Bragg peak of protons [Timlin C. and Jones B., 2010].

Proton being a charged particle just like any other charged particle with mass greater than the electron rest mass, looses energy while traversing through matter basically due to collisions with bound electrons. In these collisions an electron can either be raised to a higher shell in the absorbing atom (excitation) or it can be ejected from the atom (ionization). If the ejected electron receives enough kinetic energy, it can cause further ionizations. These electrons are referred to as δ - electrons [Kaderka R., 2011]. The energy loss per collision is typically very small, however, because of the high number of collisions per unit path length, a substantial fraction of the interacting particle's kinetic energy can be transferred to a relatively thin layer of matter [Leo W. R., 1994]. The mean energy loss per unit length for a charged particle traversing through matter is described by the Bethe-Bloch equation [Olive K. A., 2014]:

$$-\left\langle \frac{dE}{dx} \right\rangle = Kz^2\rho\frac{Z}{A}\frac{1}{\beta^2}\left[\frac{1}{2}ln\frac{2m_ec^2\beta^2\gamma^2W_{max}}{I^2} - \beta^2 - \frac{\delta(\beta\gamma)}{2} - \frac{C}{Z}\right], \tag{1}$$

where $K = 4\pi N_A r_e^2 m_e c^2 \approx 0.307\text{MeV}cm^2g^{-1}$,
and W_{max} is the maximum energy that can be transferred to a free electron in a single collision given by:

$$W_{max} = \frac{2m_ec^2\beta^2\gamma^2}{1 + 2\frac{m_e}{m}\sqrt{1+\beta^2\gamma^2} + \frac{m_e^2}{m^2}}. \tag{2}$$

Table 2.2.1 below shows the variables that are used in the Bethe-Bloch equation.

Table 2.2.1: Relevant parameters used in Bethe-Bloch equation.

Symbol	Definition	Value or unit
ρ	Density of material	gcm^{-3}
Z	Atomic number of material	
A	Atomic mass of material	$gmol^{-1}$
z	Charge number of incident particle	
β	$\frac{\nu}{c}$ of incident particle	
m_e	Electron mass	$MeVc^{-1}$
m	Mass of incident particle	$MeVc^{-1}$
c	Speed of light in vacuum	2.998 x $10^8 ms^{-1}$
γ	Lorentz factor, $\frac{1}{\sqrt{1-\beta^2}}$	
I	Mean excitation potential	eV
$\delta(\beta\gamma)$	Density effect correction	
C	Shell correction	
N_A	Avogadro's number	6.022 X $10^{23} mol^{-1}$
r_e	Classical electron radious	2.818fm
ν	Speed of incident particle	ms^{-1}
W_{max}	Maximum energy transfer in a single collision	

The mean excitation potential, I, is in essence Planck's constant, h, times the electrons average orbital frequency, ν [Leo W. R., 1994]. Using a correctly determined excitation potential is of high importance in particle therapy as the uncertainty of the excitation potential for tissues can be as high as between 5 - 15% [Andreo P., 2009] and can alter the calculated energy loss, and thereby the beam range by as much as 1.5% [Paganetti H., 2012].

The shell correction, C, is important at low energies, i.e. when the velocity of the incoming particle approaches and becomes smaller than the orbital velocity of the electrons in the absorbing material. The correction is applied in the energy range of 1 - 100 MeV, and the maximum correction is about 6% [Sengbusch E. et al., 2009]. The δ-term, i.e. the density correction, is only relevant for proton energies higher than for therapeutic purposes [Ziegler J. F., 1999, Sengbusch E. et al., 2009]. The energy loss for a heavy charged particle is highly energy dependent and is therefore mostly determined by the particle's velocity. For non-relativistic particle energies, the first term in equation (1) is predominant, and thus the energy loss has a $\frac{1}{\beta^2}$ dependence. For even lower energies, about 10MeV or less [Kaderka R., 2011], the Bethe-Bloch equation is no longer valid, and phenomenological fitting formulas and other theories are used to describe the energy loss [Olive K. A., 2014].

The amount of energy of the protons, controlling its depth, is energy dependent as it was given by the cyclotron (via acceleration). The behaviour of the proton can be precisely determined and the beam can be directed so that f energy, the proton has lost all its energy to the tissue and no primary dose is given in the exit region.Proton therapy therefore allows to target tumours inside the body, precisely localize the radiation dosage, and offering potential to greatly spare normal tissue. The depth-dose curve comparing proton and photon is as shown in the Figure 4 below.

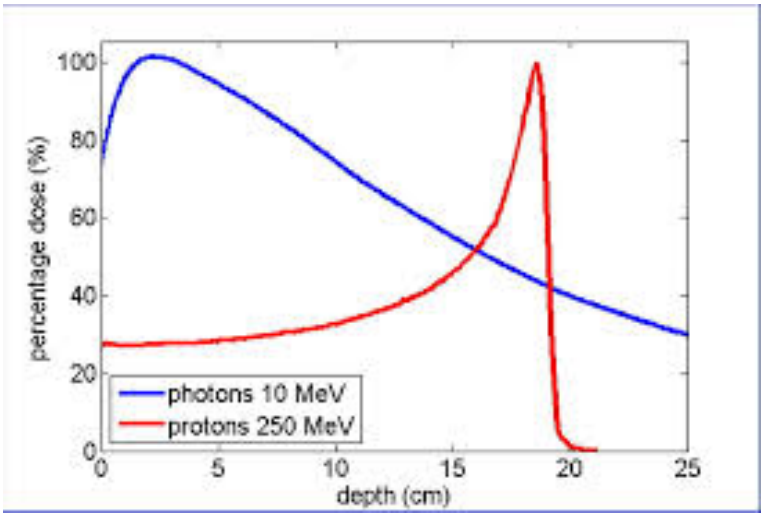

Figure 4: Depth-dose curves for protons and photons [Stephanie L. and Riesterer O., 2013].

Not all protons of the same energy have the same range due to range straggling [Paganetti H., 2012] as illustrated in Figure 5 below.

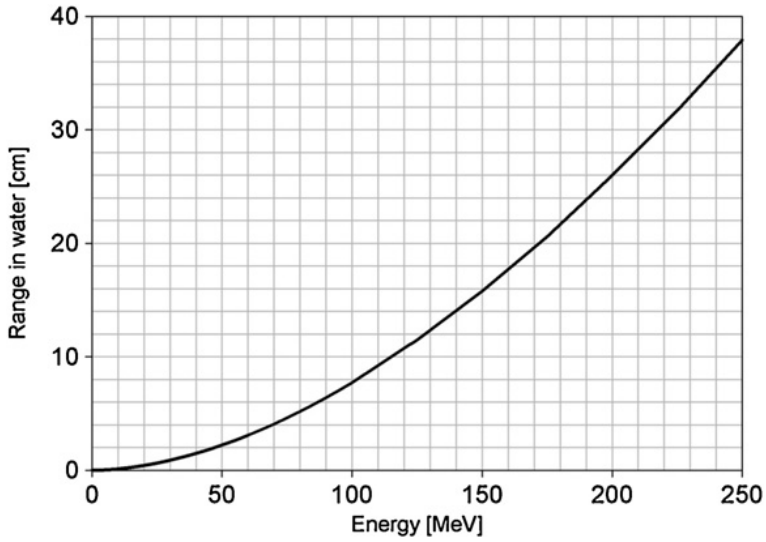

Figure 5: Energy-range relationship of monoenergetic proton beams [Paganetti H., 2012].

The range therefore needs to be defined for a beam of protons resulting in a broadened Bragg peak or a spread-out Bragg peak (SOBP) as shown in Figure 6 below.

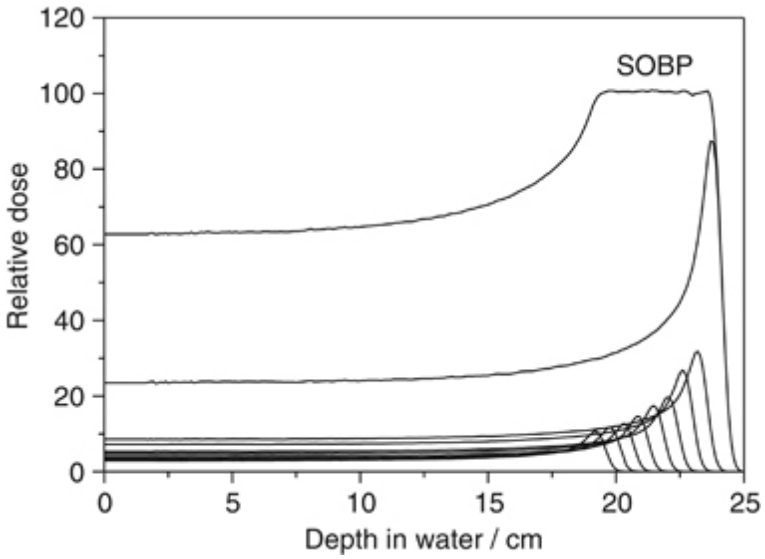

Figure 6: Illustration of SOBP [Grayden M., 2014].

The plan parameters and patient positioning must be highly precise in order to obtain a high dose within the tumor region while maximizing the protection of organs at risk (OAR). This makes the uncertainty regarding the range of motion in human tissue one of the major hurdles of RT with protons, meaning that particle therapy is more vulnerable to target motion than photon irradiation [Yoon M. et al., 2008], also describing an increased sensitivity to target motion of PBT because of deep dose depletion beyond the SOBP.

2.3 Biological effects

Ionizing radiations interacts with the living systems (cells) and affects their normal functioning. The most radiosensitive part of a cell is the DNA molecule [Saha G. B., 2006]. If the DNA is destroyed, it can lead to cell death [Borges H. L. et al., 2008].

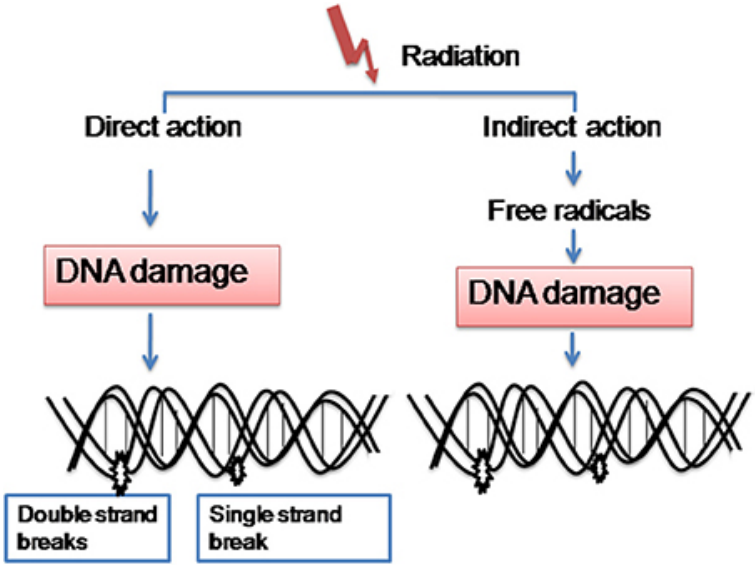

Figure 7: Direct and indirect action of radiation on DNA [Rajamanickam B. et al, 2014].

Different kinds of radiation interact with DNA molecules in different ways as illustrated in Figure 7 above. When a photon is absorbed in the cell, free electrons (δ-electrons) are produced. For radiotherapeutic energies, this happens mainly through the Compton process [Hall E. J. and Giaccia A. J., 2011]. These δ-electrons may further ionize atoms in the medium and are able to split one or two of the DNA strands if they are close enough. This type of interaction is called direct action and will in most cases lead to double-strand break (DSB). However, in photon therapy, the majority of strand breaks, i.e. about 70%, are caused by the so-called indirect action [Kelley

M. R., 2011]. In indirect action, the produced δ-electrons do not hit the DNA itself, but rather interact with water in the cells. These interactions produce a free radical, OH, which further has the ability to damage the DNA (Figure 7). The disadvantage of indirect action is that more often than not, the damage to the DNA occurs by single-strand breaks (SSB), which is easier for the cell to repair than DSBs [Saha G. B., 2006].

2.3.1 Dosimetry

Suitable units are used to determine the amount of damage to tissues due to ionizing radiation for both radiation protection purposes and radiation therapy [Cember H. and Johnson T., 2008]. This is important for the determination of the accuracy of the absorbed dose, since a small offset of the tumor dose may result into underdosage, thereby failing to control the tumor, and overdosage, may potentially result into damage to healthy (normal) tissue [Paganetti H., 2011].
It is therefore important to understand absorbed dose, equivalent dose and effective dose.

(a) Absorbed dose
Radiation damage on a tissue depends on the amount of energy deposited by radiation to the tissue. It is proportional to the mean concentration of absorbed energy in the irradiated tissue. ICRU defines absorbed dose as the mean energy imparted by ionizing radiation, ΔE, to a certain mass, Δm [Thomas D. J.,2012]:

$$D = \frac{\Delta E}{\Delta m} \tag{3}$$

The unit for absorbed dose is called Gray (Gy) in the SI system, where $1Gy = 1\frac{J}{kg}$. An important thing to remember is that the energy lost by e.g. a proton beam is larger than the absorbed dose. This is because a part of the beam's energy will be transformed into neutral secondary particles, e.g. photons and neutrons, which may deposit their energy outside the volume in question [Paganetti H., 2011].

(b) Equivalent dose
The different types of radiations have different biological effects on tissues. This difference was introduced in 1977 as the equivalent dose [ICRP, 1977]. A weighting factor, w_R, was suggested to differentiate between different particles and energies.
The equivalent dose is defined as:

$$H_T = \sum_R w_R D_{T,R} \tag{4}$$

where w_R is the weighting factor for the different radiations, as shown in Table 2.3.1, and $D_{T,R}$ is the absorbed dose averaged over the irradiated tissue(s). The unit for equivalent dose is Sievert (Sv) defined as $1Sv = 1\frac{J}{kg}$ [Mayles P. et al., 2007].

Table 2.3.1: Radiation weighting factors as defined by the ICRP Publication 103 [ICRP, 2013].

Radiation type	Weighting factor, w_R
Photons	1
Electrons and muons	1
Protons and charged pions	2
Alpha particles, fission fragments and heavy ions	20
Neutrons:	
$E_n < 1$ MeV	$2.5+18.2e^{-\frac{[ln(E_n)]^2}{6}}$
1 MeV $\leq E_n$ 50 MeV	$5.0+17.0e^{-\frac{[ln(2E_n)]^2}{6}}$
$E_n > 50$ MeV	$2.5+3.25e^{-\frac{[ln(0.04E_n)]^2}{6}}$

(c) Effective dose
Unlike the equivalent does which does not matter which tissue is being irradiated, effective dose takes into account the irradiated tissue. ICRP has introduced the effective dose where tissue

dependent weighting factors have been included [ICRP, 2013].
The effective dose is therefore defined as:

$$E = \sum_{T} w_T H_T = \sum_{T,R} w_R w_T D_{T,R}, \tag{5}$$

where w_T is the tissue weighting factor in Table 2.3.2 below and its unit is also Sv [ICRP, 2013].

Table 2.3.2: Tissue weighting factors as defined in ICRP Publication 103 [ICRP, 2013].

Organ/tissue	Weighting factor, w_T
Breast, bone marrow, colon, lung, stomach, remaining tissues*	0.12
Gonads	0.08
Bladder, liver, esophagus, thyroid	0.04
Bone surface, brain, salivary glands, skin	0.01

*Adrenals, extrathoracic region, gall bladder, heart, kidneys, lymphatic nodes, muscle, oral mucosa, pancreas, prostate, small intestine, spleen, thymus, uterus/cervix.

2.3.2 Cell survival curve and fractionation

The Linear Quadratic Model using the alpha/beta ($\frac{\alpha}{\beta}$) value describes the relationship between cell killing or cell inactivation, both for tumor as well as normal tissue in relation to prescribed dose. The dose where both the linear as well as the quadratic component cause the same amount of killing is called the $\frac{\alpha}{\beta}$ ratio. In that respect, the higher the $\frac{\alpha}{\beta}$ ratio, the more linear the cell survival curve while the lower the $\frac{\alpha}{\beta}$ ratio, the more curved the cell survival curve. The $\frac{\alpha}{\beta}$ ratio is important because tissues that have a low $\frac{\alpha}{\beta}$ are relatively resistant to low doses compared to tissues with a high $\frac{\alpha}{\beta}$. This therefore means that early responding tissues (rapidly proliferating tumors) have a high $\frac{\alpha}{\beta}$ ratio of more than 10 Gy while late responding tissues (slowly proliferating tumors) have a low $\frac{\alpha}{\beta}$ of around 3-5 Gy [Nina-Sophie Hegemann et al.]. The low $\frac{\alpha}{\beta}$ estimates for PCa suggest a greater sensitivity to increasing fraction size, raising the possibility of dose escalation through hypofractionation. The $\frac{\alpha}{\beta}$ for dose limiting organs in prostate radiotherapy is postulated to be comparatively higher (rectum and bladder; $\frac{\alpha}{\beta}$ 3 - 5 Gy). This forms the theoretical basis for an improvement in the therapeutic ratio of radiotherapy with larger fraction sizes, while delivering an isoeffective dose to the prostate [Linus C.B. et al., 2017].

The motivation behind fractionation in radiotherapy is based on the fact that there is higher repair-capacity of normal tissue compared to tumor cells, meaning there is an immediate repair of most radiation-induced sub-lethal lesions in normal tissues between the fractions and thus allowing a relative tumor-specific therapeutic effect [Fowler J. F. et al., 2010].
The optimal radiation schedule for the curative treatment of prostate cancer is not known [Brenner D.J., Hall E.J., 1999]. Prostate cancer patients receiving external beam radiation therapy (EBRT) typically are treated 5 days per week using daily dose of 1.8 - 2.0 Gy over 7 - 8 weeks, to a total dose of 74 - 79.2 Gy [Zietman A. et al., 2001]. Based on recent data some clinicians have increased the total dose of radiation by increasing the number of treatment sessions or fractions and it is now the standard at some centers to treat men for 8 - 10 consecutive weeks [Zelefsky M.J. et al., 2002]. The dose of 1.8 - 2.0 Gy per fraction in conventional fractionation (CF) is based on the presumed relative sensitivity of malignant and normal tissue.

2.3.3 Relative Biological Effectiveness (RBE)

Particles , compared to photons , have a greater radiobiological effect and, therefore, greater potential to damage cancer cells by interacting more densely with tissue, causing higher levels of ionization per unit length. The dose then rapidly decreases to zero as heavy particles (as opposed to photons) stop within the body. Therefore, the integral dose with protons is approximately 60% lower than that of an external beam photon technique. In order to benefit from the extensive experience from photon treatments, proton therapy prescriptions are based on physical dose times a factor to account for the difference in biological effect at the same dose when treating with photons. This is described by the relative biological effectiveness (RBE); the ratio of doses to reach the same level of effect (i.e. EndpointX) when comparing two radiation modalities, in this

case, a reference radiation and proton radiation (Equation 6).

$$RBE(Dose, EndpointX, proton\ beam\ properties) = \frac{Dose_{reference}(EndpointX)}{Dose_{protons}(EndpointX)} \tag{6}$$

The dose in proton therapy is prescribed as Gy[RBE] according to the International Commission on Radiation Units and Measurements [ICRU 2007] and in this thesis, we shall use only Gy instead of Gy[RBE] for simplicity. We use Gy[RBE] but we denote it by Gy. So, whenever Gy is used, we mean Gy[RBE] (the factor 1.1 is already accounted for in the treatment planning system). Typically, all treatments in proton therapy assume an RBE of 1.1, a value which is primarily based on animal experiments conducted in the 1970s [Paganetti H., 2015]. However, the RBE varies depending on a particle's energy, depth of penetration, dose per fraction and other parameters [Paganetti H., 2011]. The single value of 1.1 is therefore only a generic value. It has been shown in in vivo and in vitro studies that the RBE can vary significantly [Paganetti H. et al., 2002], but there is no clear clinical data that indicates that the use of 1.1 as the generic RBE value is unreasonable [Paganetti H., 2014]. In addition, there is no clear clinical data that confirms that an RBE of 1.1 is correct [Paganetti H., 2011]. The RBE is closely related to the LET in the sense that the former increases as the latter increases. At a LET of approximately 100 keVμm^{-1}, the maximum RBE is about 3-8, depending on the level of cell kill. Beyond this LET value, the RBE declines due to cell overkill. This is because high LET particles are densely ionizing and will deposit more energy to the DNA than what is required to kill the cell, thereby decreasing the effectiveness. This effect is shown in Figure 8 below.

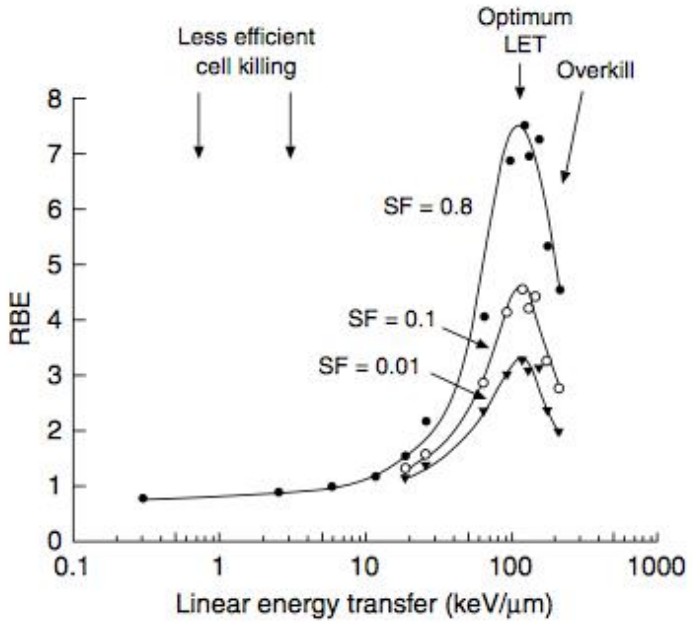

Figure 8: Illustration of the relationship between RBE and the mean LET. [Mayles A. et al., 2007].

2.4 Photon Therapy Techniques

A number of techniques are employed in the delivery of photons for the treatment of cancer. The delivery is by use of a LINAC which is a device that uses electricity to form a stream of fast-moving subatomic particles (photons or electrons). This creates high-energy radiation that may be used to treat cancer.

The LINAC uses microwave technology to accelerate electrons in a part of the accelerator called the wave guide which allows these electrons to collide with a heavy metal target to produce high-energy x-rays. These high energy x-rays are then shaped as they exit the machine to conform to the shape of the tumor and the customized beam is directed to the tumor. The beam is usually shaped by a multileaf collimator (MLC) that is incorporated into the head of the machine. The patient lies on a moveable treatment couch and lasers are used to make sure the patient is in the proper position. The treatment couch can move in many directions including up, down, right, left, in and out. The beam comes out of a part of the accelerator called a gantry, which can be rotated around the patient. Radiation can be delivered to the tumor from any angle by rotating the gantry

and moving the treatment couch. Patients usually receive EBRT in daily treatment sessions over the course of several weeks. Figure 9 below shows the major components of a LINAC.

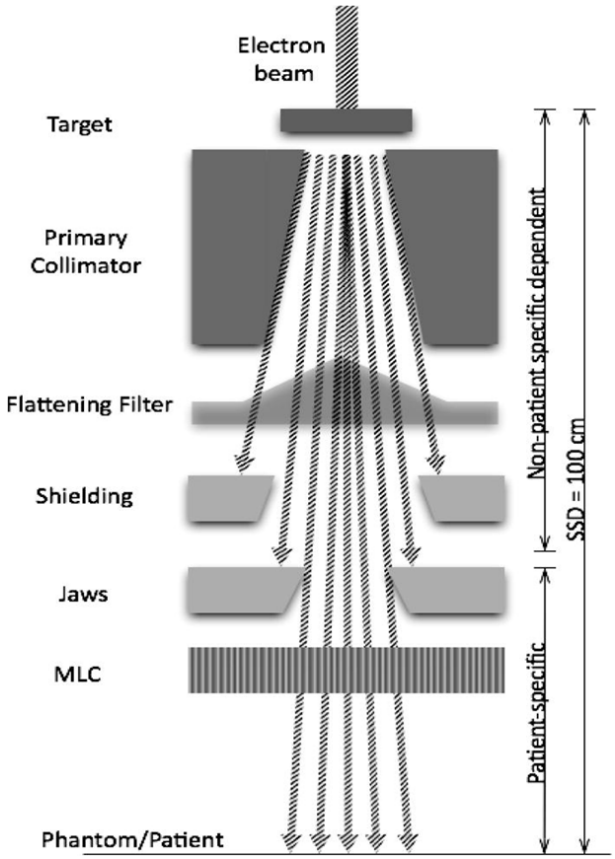

Figure 9: Schematic overview of the simulated Varian Trilogy LINAC head [Borges C., 2011].

A LINAC can be used in a number of ways to carryout the treatment as discussed below:

2.4.1 Three-dimensional conformal radiation therapy (3D-CRT)

Here treatment is achieved by conforming the shape and size of the beam from the LINAC by the MLCs to that of the tumor/target volume. It is therefore challenging when the target volume is complex/non-uniformly shaped and is near to or wrapped around an organ at risk (OAR). This makes it difficult to conform the dose to this shape resulting into the portion of the OAR immediately surrounding the target to receive high dose. A solution to this could be to use a series of sequential phases which enables delivery of high dose to the primary site and a lower dose to areas close to OAR [James A.P., 1999].

2.4.2 Intensity Modulated Radiotherapy (IMRT)

IMRT works by varying the dose intensity across the beam and this enables tailoring of the dose distribution more precisely to the shape of the target. Intensity across the beam is achieved by using the multileaf collimators (MLCs), which move into different positions throughout the delivery of the beam, shielding some areas within the field more than others. This can be done by dynamic motion of the MLCs where the MLCs move across the beam at different speeds to build up areas of low and high intensity or step and shoot motion where each beam angle consists of sub-fields which are delivered sequentially. In the stop and shoot, The machine is only switched on for each sub-field once the MLCs are in the correct position, and switched off and the leaves will move to the next position [Craig E., 2011].

2.4.3 Volumetric Arc Radiotherapy(VMAT)

Variation of IMRT is called VMAT and LINAC is used as it delivers the radiation quickly when the gantry rotates once around the body and the treatment is given over just a few minutes. In VMAT, there are no set beam angles, the intensity modulated beam is deliverd as the gantry arcs

around the patient, that is the beam is dynamically delivered. The gantry speed adds a further dynamic component that can be used to control the intensity of the beam as needed [Erminia I., 2015].

2.5 Proton Therapy Techniques

Protons can be generated/delivered by a special machine called a cyclotron or synchrotron. This machine costs millions of dollars and requires experts to use and maintain it. Because of this, proton beam therapy is expensive, and very few treatment centers in the United States, Germany, Sweden, but many countries are currently building new facilities (Netherlands, Denmark, etc). In order to achieve the prescribed dose to the prescribed area, different types of equipment are used to direct and shape the beam. A monoenergetic beam from the accelerator is unsuitable for cancer treatment due to its longitudinally narrow Bragg peak. In order to cover the target volume in its full depth, beams of decreasing energy, and typically decreasing weight, are combined to create the spread-out Bragg peak (Figure 5). This can be done either actively or passively [Paganetti H., 2011].

(a) Active modulation
Active modulation is only possible for synchrotrons. This involves the direct change of the energy of the beam within the accelerator and the energy change must happen quickly in order to limit the treatment duration and to allow for fast switching between treatment rooms. The energy selection must also be accurate in order to determine the depth of the Bragg peak with sufficient accuracy [Paganetti H., 2011].

(b)Passive modulation
Passive modulation is used for cyclotrons only. This is because these accelerators only work at a specific energy. Passive modulation is achieved by inserting material in front of the beam, thereby decreasing the effective energy, and thus the range of the particles. This can either be done immediately after the beam has been extracted from the cyclotron, or the modulation can take place directly inside the treatment nozzle [Paganetti H., 2011]. To create the SOBP, either a plate with ripples (ridge filter) or a rotating wheel with varying thickness in the azimuthal direction (modulator wheel) is used. The modulators are designed such that the result is a predefined depth dose profile.

2.5.1 Beam delivery

Both longitudinal and lateral dose spread over the target is required during the course of beam delivery which can be done by different beam delivery techniques. There are two major delivery techniques in particle therapy: beam scanning (active beam shaping) and beam scattering (passive beam shaping) [Schulz-Ertner D. et al., 2006].

(a)Passive scattering
This was the first method to be developed. In this delivery technique, the narrow particle beam is spread in the lateral direction either by using one scatter foil (single scattering technique), when small fields are requested, or two scatter foils (double scattering technique), when a broader beam is preferable [Schippers J. M., 2009]. The beam must additionally be shaped according to the target volume. Collimators are used to adapt the field for each separate treatment angle [Paganetti H., 2011]. Figure 10 shows passive scattering.

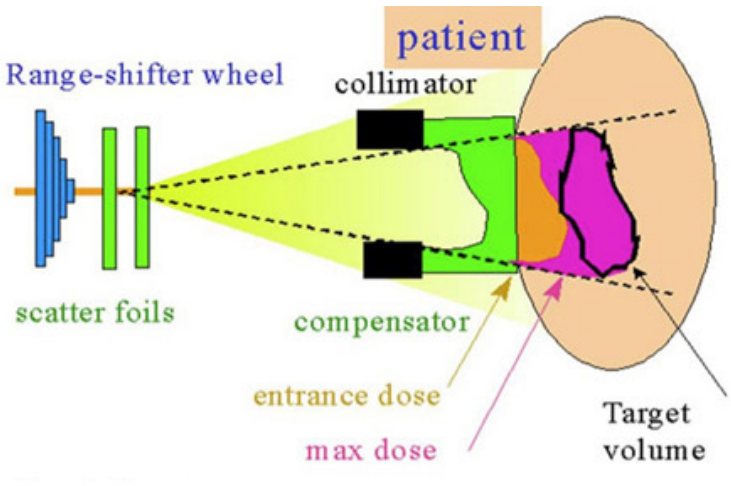

Figure 10: Illustration of passive scattering [Carolyn V., 2015].

The main advantage of passive scattering is that the change of energy between the different layers is achieved much faster than the scanning technique. Since the whole field is delivered almost at once, the complete treatment duration will also be shorter [Engelsman M., 2013]. However, in passive scattering technique, subsidiary dose to the patient may occur due to the additional collimation material in the beam line and this can lead to more nuclear fragments [Paganetti H., 2011].

2.5.2 Scanning beam

Pencil beam scanning uses magnets to deflect, focus and steer the charged particles in the beam. The magnets consist of two dipoles, run by fast power suppliers; one for horizontal steering and one for vertical steering. This way a narrow beam can be used to "paint" the dose over the target, layer by layer. When one layer of voxels has been irradiated, the energy of the beam is decreased, and a new layer can be treated [Grupen C. et al., 2011]. The voxels, or spots, can be irradiated one by one (discrete spot scanning) meaning that the beam is turned off between the irradiation of each spot. Another method is the raster scanning technique where the beam continuously irradiates while the dipoles are simultaneously steering the beam [Schippers J. M., 2009]. In pencil beam scanning, it is highly important that beam intensities and beam positions are monitored in order to ensure a safe and accurate delivery of the dose to the patient [Schlegel W.C. et al, 2006]. The main advantage of pencil beam scanning is that it has a high dose conformity compared to the passive scattering technique, and hence, lower doses to healthy tissues may be achieved. There will also be no additional dose due to nuclear fragmentation from beam shaping materials [Paganetti H., 2011]. The method of pencil beam scanning is shown in Figure 11 below.

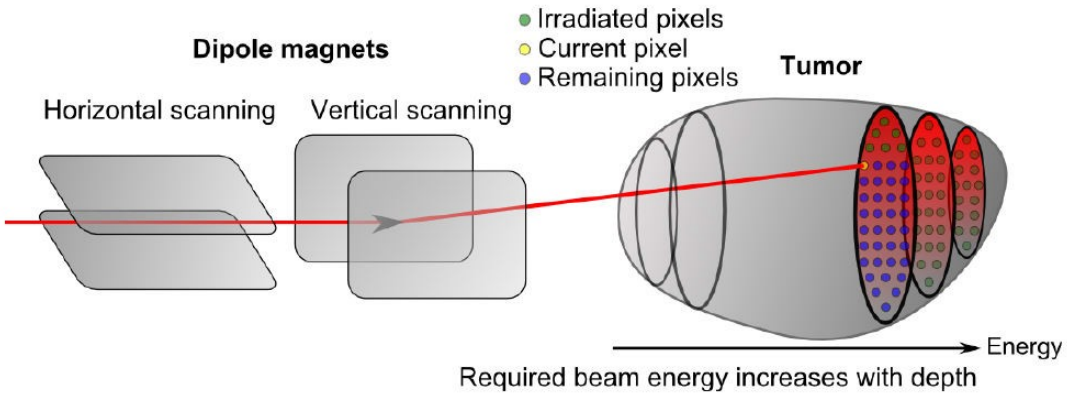

Figure 11: Illustration of pencil beam scanning [Paganetti H., 2011].

Proton pencil beams relies on the charged-particle Bragg peak.This means the use of characteristic peak of dose at the end of range together with the modulation of pencil beam variables to create target-local modulations in dose that achieves the dose objectives. IMPT makes better the X-ray intensity modulated beams (intensity modulated radiotherapy or volumetric modulated arc therapy) with dose modulation along the beam axis and also lateral, in-field, dose modulation. IMPT is therefore the electromagnetic spatial control of well-circumscribed pencil beams of protons of variable energy and intensity. It has an disadvantage that the treatment takes longer than with passive scatter.

Chapter 3: Treatment planning and strategies for treatment delivery

3.1 Patient model

In the process of image acquisition using any modality such as CT, MRI to be used in the treatment planning system (TPS) there has to be a reproducible patient positioning. These images are used to define and display contours and surfaces for normal and critical structures. Registration of all input data, including registration with initial simulation contours, films, patient position, etc are then done to enable define target contours, generate 3D target surface using surface expansion, import target information from multiple imaging modalities. This is then followed by determining beam or source arrangements, generating beam's-eye-view displays. If need be design of field shape using blocks, MLC; determine beam modifiers using compensators, wedges and determine beam or source weighting. With all these in place then selection of dose calculation algorithm and methodology, calculation grid and window, etc are done and sequentially dose calculations, relative and absolute dose normalizations and input of the dose prescription. To estimate dose, Hounsfield units (HU) are converted to electron density/stopping potential and that is why HU is a common unit used to express CT numbers in a standardised and convenient form in CT.

3.2 Geometrical uncertainties

High geometrical accuracy is a prerequisite for a safe clinical application of conformal RT [Marcel Van Herk, 2004]. However, treatment optimization is limited by variation in delivered dose caused by errors in patient treatment positioning and interfractional variation of organ position, size, and shape.

An error in photon and proton therapy refers to any deviation between planned and delivered dose. There are two types of errors that are encountered; random and systematic errors. Random errors are treatment execution errors and influence each fraction individually while, systematic errors are treatment preparation errors and influence all fractions.

There are a number of causes of these errors at the treatment planning stage; for instance, motion of skin with respect to the internal anatomy which limits the reproducibility hence introducing a systematic setup error. The tumor is imaged in an arbitrary position which leads to a systematic error and this may further lead to the image being distorted because of the interference of the scanning process and organ motion. Delineation during treatment planning is also another process that may introduce systematic error. Random errors also occur during treatment and these errors are mostly due to setup error and organ motion. In this study, motion uncertainity is of interest and motion can be divided into inter- and intrafractional movements. Interfractional movements are variations occurring between two different fractions e.g, due to daily variation in filling of the bladder and rectum. Intrafractional movements happen within a treatment session, e.g, due to breathing, bowel gas, or small patient movements. These movements result into setup error which has both a systematic and a random component. For instance, motion of skin with respect to the internal anatomy limits the reproducibility of the patient setup on the CT scanner, introducing a systematic setup error. Variations in daily setup may affect the target coverage [Zhang X. et al., 2007, Yoon M. et al., 2008, Sejpal SV. et al., 2009].

3.3 Methods to account for motion uncertainties in delivery

The patient is fitted with immobilisation device such as knee cushion, feet board to keep the body part to be treated still during treatment. At the beginning of the treatment session, the therapist positions the patient on the treatment table, guided by the marks on the skin defining the treatment area. If molded devices were made, they will be used to help the patient maintain the proper position. The patient may be repositioned during the procedure. Imaging systems on the treatment machine such as x-ray or CT may be used to check positioning and marker location.

3.3.1 Estimation of margins to account for motion

Systematic and random errors have different significant dosimetrical impacts, and should be treated differently in margin calculations [Stroom J.C. et al., 2002]. This means that random and systematic errors, Σ_{pop} and Σ_{pop} should not be added in quadrature to determine the margin.
CTV to PTV margin (M) recipe that properly accounts for the different consequences of systematic and random errors were proposed in 1999 [Stroom J.C.et al, 1999]. Basing on the calculation of

DVHs, it was found that $M = 2\Sigma_{pop} + 0.7\sigma_{pop}$ ensured adequate coverage of CTV. The assumption for the derivation of the recipe was that, on average, 99% of the CTV should at least get 95% of the dose which was derived from ICRU criterion [Stroom J.C.et al, 2002]. $M = 2\Sigma_{pop}$ was used for systematic error and the average DVH represented each patient's situation fairly well with only a small inter-patient variation [Stroom J.C.et al, 2002].
Using average histograms of similar type (minimum dose-population histograms), a similar margin by Stroom et al. was proposed, $M = 2.5\Sigma_{pop} + 0.7\sigma_{pop}$ [Van Herk et al., 2000]. The assumption for the recipe was that for 90% of the patients, the minimum dose should be at least 95%.

3.3.2 Image-guided radiation therapy (IGRT)

There is no standardized or consensus definition of IGRT. It has been rather malleable and author dependent, meaning different things to different people [Gupta T. and Anand N.C, 2012]. Some define it very broadly i.e., use of imaging for detection and diagnosis; delineation of target volumes and organs-at-risk (OARs); determining biological attributes such as size, shape and position of the tumor; dose distribution design; dose delivery verification and assurance; and deciphering treatment response [Reco C. et al., 2008]. A more focused and accepted definition of IGRT is use of frequent imaging within the radiation treatment room, with decisions based on imaging to improve precision of radiation therapy delivery i.e., process of in-room imaging guiding radiation delivery [Verellen D. et al., 2008, Dawson L.A. et al., 2007]. Imaging includes but may not be limited to planar imaging, cine-imaging, volumetric imaging and surface-tracking [Gupta T. and Anand N.C, 2012].

3.3.3 Adaptive Radiation (Proton) Therapy (ART or APT)

Adaptive radiotherapy is defined as changing the original radiation treatment plan (by modifying either beam apertures or intensity patterns) during a course of fractionated radiotherapy to account for the temporal changes in anatomy (weight loss, tumor shrinkage, internal organ motion) or changes in tumor biology or function (hypoxia, proliferation) [Yan D. et al., 2010]. It aims to adapt to the change in patient contour or tumor volume by modification of the dose prescription, target volumes, and/or the treatment plan. A novel method of adaptive planning is to make multiple plans for predictable change in the shape and size of target volumes with treatment being executed with the 'plan of the day' that most fits the changing anatomy [Gupta T. et al., 2012].

Adaptive radiotherapy has been introduced to either reduce or compensate for the effect of patient-specific treatment variation measured during the course of radiotherapy. Adaptive radiotherapy help to manage an individual's treatment by, including patient-specific treatment variation identified and quantified during the course of radiotherapy in the treatment planning and delivering optimization. The importance of using an adaptive process in radiation therapy is that the treatment plan, especially the margin and treatment dose, can eventually be customized to the individual patient. Studies have demonstrated that adaptive radiotherapy could significantly improve the therapeutic ratio by safely reducing the large target margin that has to be used in conventional radiotherapy for prostate cancer treatment [Michel G. et al., 2010]. Clinical application of off-line image-guided adaptive radiotherapy for prostate cancer has demonstrated encouraging clinical outcome [Michel G. et al., 2010]. Long-term clinical follow-up has shown significant improvement in terms of tumor control and low toxicity profile, emphasizing the beneficial effect of image-guidance and adaptive treatment [Michel G. et al., 2010]. Continuous development in adaptive radiotherapy has made possible additional increases in target dose by further reducing target margin when using on-line image-guided adaptive intensity-modulated radiation therapy.

3.3.4 Definition of target volumes

Different volumes related to both the tumor and the normal tissues are defined for use in the treatment planning and evaluation processes. These different volumes are delineated in the planning process and are used for prescription, recording and reporting doses to the target volumes and volumes of normal tissues at risk [ICRU report 83, 2010]. These volumes include: gross tumor volume (GTV), the clinical target volume (CTV), the planning target volume (PTV), organ at risk (OAR), planning organ at risk volume (PRV), internal target volume (ITV), treated volume (TV) and remaining volume at risk (RVR). The important volumes that will be referred to for the purpose of this study are; CTV, PTV and OAR.

(a) Gross tumor volume (GTV)
GTV refers to the gross demonstrable extent and location of the tumor. The GTV may comprise

of a primary tumor (primary tumor GTV or GTV-T), metastatic regional node(s) (nodal GTV or GTV-N), or distant metastasis (metastatic GTV or GTV-M).
GTV needs to be described and reported completely and accurately for a number of reasons;
Firstly, GTV is a requirement in staging of the tumor. Secondly, to obtain a local tumor control, an adequate absorbed dose must be delivered to the whole GTV. The third reason is that, the evaluation of the regression of the GTV might be needed for redefining the CTV and the PTV during the course of treatment. Fourthly, changes of GTV during treatment might be predictive of treatment outcome [ICRU report 83, 2010].

(b) Clinical target volume (CTV)
The CTV is a volume of tissue that contains a demonstrable GTV and/or subclinical malignant disease with a certain probability of occurrence considered relevant for therapy. There is no general consensus on what probability is considered relevant for therapy, but typically a probability of occult disease higher than from 5% to 10% is assumed to require treatment [ICRU report 83, 2010]. The selection of the tissues that bear risk for microscopic infiltration outside of the GTV is a probabilistic assessment integrating the biological and clinical behavior of the various tumor entities and the knowledge of the surrounding anatomy, including structures that are barriers to tissue infiltration (e.g., muscular fascia, bone cortex), or on the contrary - structures that are easy conduits for tumor dissemination (e.g., fatty space). Different tumors can exhibit a variety of spread patterns [ICRU report 83, 2010].

(d) Planning target volume (PTV)
The PTV is a geometrical concept introduced for treatment planning and evaluation. It is the recommended tool to shape absorbed-dose distributions to ensure that the prescribed absorbed dose will actually be delivered to all parts of the CTV with a clinically acceptable probability, despite geometrical uncertainties such as organ motion and setup variations. It is also used for absorbed-dose prescription and reporting. It surrounds the representation of the CTV with a margin such that the planned absorbed dose is delivered to the CTV [ICRU report 83, 2010].

(e) Organ at risk (OAR)
The OAR or critical normal structures are tissues that if irradiated could suffer significant morbidity and thus might influence the treatment planning and/or the absorbed-dose prescription. In principle, all non-target tissues could be OARs. However, normal tissues considered as OARs typically depend on the location of the CTV and/or the prescribed absorbed dose. For example, in the post-operative irradiation of a lower-limb soft-tissue sarcoma, the muscles that are not included in the compartment at risk for microscopic infiltration are considered as OARs, and thus will influence the beam delivery [ICRU report 83, 2010].

(f) Planning Organ at Risk Volume (PRV)
Just like in the case of the PTV, uncertainties and variations in the position of the OAR during treatment must be considered to avoid serious complications. This therefore means margins have to be added to the OARs to compensate for these uncertainties and variations, using similar principles as for the PTV. This leads, in analogy with the PTV, to the concept of PRV [ICRU report 83, 2010].

3.3.5 Treatment planning

Dose volume histograms (DVHs) are a simple way to evaluate the dose distribution on volumes of interest. Cumulative DVHs, showing the amount of dose up to a given value received by a fraction of the total volume, are the most common type of dose volume histograms. The DVHs can employ both relative and absolute doses and volumes. By using DVHs for plan assessment and comparison, the spatial information is lost. This loss of spatial information can, however, be compensated for by using dose distribution displays in conjunction with the DVHs [Li Z., 2009].
Absorbed dose is used in the formulation of objective functions in optimization systems. Although dose volume histogram (DVH) - objectives are notoriously difficult to handle in the optimization process [Clark V. H. et al., 2008], progress towards an efficient reformulation of the problem has been made [Zarepisheh et al., 2013]. Since DVHs are widely used for clinical assessment of dose plans, they would have an immediate effect both on treatment plan optimization and quality assurance, if it is possible to predict what DVHs are achievable.

The method of inverse planning is typically used for intensity-modulated particle therapy

(IMPT). IMPT in pencil beam scanning means that the scanning magnets can steer the pencil beam and conform the dose in the transverse plane. Dose conformation in this plane is also achievable for photons by IMRT or VMAT. However, due to the Bragg peak of protons, an additional degree of freedom is introduced, meaning that modulation along the beam axis is possible. In IMPT, each pencil beam must be weighted relative to each other and must be optimized separately [ICRU report 78, 2009]. The optimization process is an important part of the treatment planning. Optimization is essentially to iteratively generate, followed by automatically assessing, a large number of plans and choosing the best among them. A computer is given constraints and objectives on targets and organs at risk by a clinician. If given constraints, the computer must follow these without violation. Objectives, on the other hand, are typically given weights relative to each other, in which case a small violation may be allowed. An example of objectives can typically be 51Gy to 0% of the tumor volume, while no more than 49Gy should be received by 100% of a nearby OAR. When the computer have calculated the best plan for the given constraints, it should be inspected by the treatment planner. If the results are unsatisfactory, the objectives and constraints can be edited and a re-optimisation can be done.

3.4 Plan evaluation-DVH and how evaluation criteria has been derived

A treatment plan is evaluated by several different methods. Usually, dosimetrics and volumetrics are inspected using dose distributions displayed onto patient CT scans, and graphically using DVHs alongside predetermined dose constraints to target volumes and organs at risk [Li Z., 2009]. Objective functions are commonly used in radiotherapy to measure treatment plan quality and can be classified into physical, e.g., the minimum/maximum dose and mean dose, and radiobiological, e.g., the equivalent uniform dose (EUD), tumor control probability (TCP), normal tissue complication probability (NTCP) and logarithmic tumor control probability (LTCP). The first class typically measures deviations from a prescribed dose level in an organ, while the second class attempts to model the radiobiological effects of irradiating the organ.

3.5 Robust evaluation

Target coverage should generally not be compromised to reduce the normal tissue risks when doing plan evaluation. The quality of a treatment plan is evaluated in several ways by looking at outcomes of treatment quantities such as DVH parameters, tumor control probability (TCP) and normal tissue complication probability (NTCP) or equivalent uniform dose (EUD) [Niemierko A., 1999]. Due to the non-uniform nature of dose distributions throughout organs or volumes, it is always difficult to report the doses by use of some parameters like dose volume distributions/histograms (DVD/DVH). Equivalent uniform dose (EUD) is used for reporting and quantitatively compare in-homogeneous dose distributions. EUD is the dose (in Gy), which, when distributed uniformly across the target volume, causes the survival of the same number of clonogens [Niemierko A., 1997].

Range uncertainties are simulated by recalculating the treatment plans on a repeat CT scan where all CT numbers are systematically increased or decreased by a given percentage of its value, as proposed by Lomax et al. [Lomax et al., 2008]. Setup uncertainties can be simulated by an online patient setup correction protocol with bony anatomy as reference. Ideally, setup errors are zero after applying online corrections. But not all errors are eliminated for instance, errors from intrafractional motion or uncorrected deformations of the bony structures [Van Kranen S., 2009].

Chapter 4: Project aim and motivation

The aim of this project is to construct a plan library of the lymph nodes with prostate at different positions to help investigate if the construction of a plan library for prostate cancer patients can result in improvement of dose to the tumor while reducing the doses to the surrounding normal tissues and OARs. The involvement of three target structures; prostate, seminal vesicles and lymph nodes; and the independent motion of these structures make delivery of the treatment with protons challenging and therefore use of plan library could improve on the dose on the target while sparing the normal tissues.

A plan library approach has been employed in one previous study for photons [Xia P. et al., 2010], but this thesis will extend it to proton therapy. Due to the nature of how proton deposits its energy, we think that by establishing the appropriate margins and using appropriate plan-of-the day, this strategy will lead to improved doses to the targets and reduced doses to the OARs near the targets. Furthermore, this method could be one of the simple feasible methods as we shall have only one planning CT (pCT) per patient and no delineation of the target volumes is required for every treatment session. As mentioned earlier, RT of prostate is challenging as there are internal target and organ motion during treatment. To limit range uncertainties, we shall employ bony anatomy setup in this study basing on a study conducted by Th*ö*nqvist S. et al. which showed that bony anatomy setup was slightly better compared to positioning using fiducial markers [Th*ö*nqvist S. et al., 2013]. The plan library will be limited to three plans in addition to one conservative plan with larger margins and this will allow feasibility for manual selection otherwise manual selection will become difficult with large number of plans. Finally, the plan library construction will be based on a population analysis of prostate motion relative to bony anatomy, and thus will require only a single pCT for every patient.

Chapter 5: Method and materials

This chapter gives the details of the method and materials employed in this master project for two studies A and B. Study design, patient selection, patient material and how the studies were carried out will be described including the variables considered as well as the analysis.

5.1 Study design

The study was designed as a quasi-experimental retrospective study using acquired image information of patients previously treated at Haukeland University Hospital. The study was focused on method-development for treatment of locally advanced prostate cancer with intensity-modulated proton therapy (IMPT) and compared two different treatment options by in-silico simulation of delivered dose based on repeat imaging (CT) data of each individual patient.
The study was divided in two phases:
(A) An initial analysis of prostate target motion relative to bony anatomy and;
(B) Comparison of two different treatment options. The results from the initial analysis (A) were used as input for (B).

5.2 Patient selection

The patients selected for inclusion in this study had a number of criteria that were fulfilled as mentioned below. All these patients;

- had locally advanced T2-T4 prostate cancer, Nx-1, M0, PSA $>$ 10 and Gleason score $>$ 7.
- had fiducial gold markers implanted into the prostate gland.
- were treated during 2007/2008 at Haukeland University Hospital as a part of a phase II dose-escalation trial (REK approval 2006 -15727 IMRT basert integrert boost ved lokalavansert cancer prostate En fase II studie).
- had repeat CT (rCT) scans acquired twice a week during the course of treatment for the purpose of studying organ motion and development of new treatment techniques for compensation of geometrical uncertainties.
- had signed written consent for participation in the study including acquisition of rCT scans.

Eighteen (18) patients meeting the inclusion criteria were used in the initial analysis, A of inter-fractional prostate target motion relative to bony anatomy. Five (5) independent patients meeting the inclusion criteria and not included in the initial analysis were then used for comparison of the two different treatment options B. These patients furthermore had CTVs and OARs contoured and quality checked by an independent observer on all rCTs.

The number of patients was chosen as a trade-off between sufficient data for statistical analysis and manageable workload within the time frame of the master thesis project.

5.3 Patient material

For the selected patients, CT images had been acquired and volumes contoured as described in the following sections.

5.3.1 CT scanning

All the twenty three (23) patients had undergone CT imaging. The planning CTs (pCTs) were acquired with bladder contrast while the rCTs were acquired without bladder contrast but with same protocol as in the pCT acquisition. The rCTs were acquired twice a week during the course of treatment, as close to the treatment session as practically as was possible. All CTs were acquired with knee and ankle fixation in place in the head-first-supine position and covered L3/L4 to anus. Before the acquisition of the pCT, no laxatives were given to the patients but they were asked to empty their bowels before the pCT was taken. A total of 225 CTs from the twenty three patients were obtained with each patient having one pCT and a range of 6 - 10 rCTS.

5.3.2 Gold marker (GM) based registrations

For each patient, each of the rCTs had been registered to the pCT based on the fiducial gold markers (GM) implanted into the prostate. This had been performed by a medical physicist in Eclipse Treatment Planning System (Varian Medical Systems, Palo Alto, CA, USA) uisng a manual procedure allowing for translational shifts only.

5.3.3 Contouring

Manual contouring had been employed for all the three different targets. The manual contouring on pCTs and all the rCTs were done in Eclipse Treatment Planning System (Varian Medical Systems, Palo Alto, CA, USA). The delineation was such that CTV67.5 was defined as the prostate gland including the capsule as well as tumor extension outside the prostate gland, CTV60 overlapped with CTV67.5 and also included the seminal vesicles and CTV50 was defined as CTV60 and the pelvic lymph nodes contoured according to the Radiotherapy Oncology Group (RTOG) guidelines but omitting the pre-sacral nodes. All these target volumes had been contoured by the same experienced oncologist.

Other organs contoured included the rectum which was defined from the recto-sigmoid flexure to the anal verge including content and the bladder which was defined from apex to dome including content. The contouring of both the rectum and the bladder on all CT scans for all patients had been done by a single medical physicist. Large bowel was contoured from the recto-sigmoid flexure and up to L3/L4 and small bowel was contoured as the remaining bowel loops and this had been done by a single medical physicist. Quality assurance of all the contouring had been done by an independent medical physicist.

5.4 Registration on bony anatomy (BA)

Registration of the rCTs to the pCT was performed for each individual patient (23 patients in total) to mimic image-guided patient positioning based on bony anatomy. This was performed by the candidate using the image registration software implemented in Eclipse TPS (Varian Medical Systems, Palo Alto, CA, USA). The registrations were restricted to rigid translational shifts in the Right-Left (x), Anterior-Posterior (y) and Caudal-Cranial (z) directions and performed according to procedure (Appendix A). Automatic registration was employed here, but a coarse manual registration was performed beforehand to roughly align the CT datasets. Subsequently, a volume of interest (the registration box) was placed around the pelvic bones including the prostate to restrict the registration area. Finally, the result of the automatic registration was visually reviewed to exclude obviously inaccurate registrations and re-registrations were done for the inaccurate ones. Accurate registration is one where visual inspections reveal that the rCT is lying exactly on top of the pCT as explained in Appendix A.

5.5 Study A: Prostate target motion relative to bony anatomy

5.5.1 Aim

The aim of this study was to determine the degree of interfractional prostate motion relative to bony anatomy which will then be used to calculate population based margins to be used as margins to create PTVs for study B and hence the input for constructing a plan library.

5.5.2 Variables

The x-, y- and z-coordinate vectors of the registrations based on both the GM and BA were recorded in millimeters (mm) . These registration coordinate vectors were based on DICOM/Eclipse coordinate system and were used to calculate the magnitudes and directions of the shifts of the prostate in the respective directions for each rCT for all the 18 patients as illustrated in Figures 12 and 13 below.

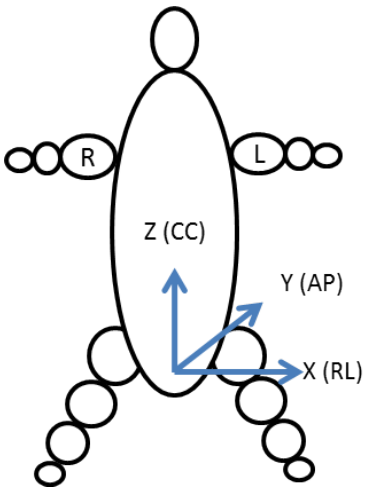

Figure 12: Eclipse coordinate system with the patient lying in "head-first-supine" position.

x - from right to left (RL)
y - from anterior to posterior (AP)
z - from caudal to cranial (CC).

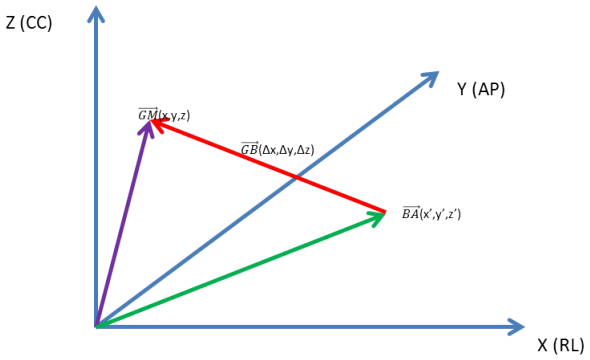

Figure 13: Illustration of registration vectors and how the shift, $\vec{GB}$ was calculated from gold marker-based ($\vec{GM}$) and bony anatomy-based ($\vec{BA}$) registration vectors.

The shift between gold marker-based registration and bony anatomy-based registration was calculated as;

$$\vec{GB}(\Delta x, \Delta y, \Delta z) = \vec{GM}(x, y, z) - \vec{BA}(x', y', z'), \tag{7}$$

where $\vec{GM}(x, y, z)$ was the GM based registration coordinate vector, $\vec{BA}(x', y', z')$ was the BA based registration coordinate vector and $\vec{GB}(\Delta x, \Delta y, \Delta z)$ were the shifts in the respective directions.

$\vec{GB}(\Delta x, \Delta y, \Delta z)$ was calculated for each patient j ($j \in [1, N]$) and each rCT i ($i \in [1, K]$); and was used to calculate the systematic error for patient j, $\mu_j(\Delta x)$ in x (Δx), $\mu_j(\Delta y)$ in y (Δy) and $\mu_j(\Delta z)$ in z (Δz) directions as,

$$\mu_j(\Delta x) = \frac{1}{K} \sum_{i=1}^{K} \Delta x_i \ , \tag{8}$$

$\mu_j(\Delta y)$ and $\mu_j(\Delta z)$ were calculated the same way.
$\vec{GB}(\Delta x, \Delta y, \Delta z)$ was also used to calculate the random error for patient j, $SD_j(\Delta x)$ in x (Δx), $SD_j(\Delta y)$ in y (Δy) and $SD_j(\Delta z)$ in z (Δz) directions as,

$$SD_j(\Delta x) = \sqrt{\frac{1}{K-1} \sum_{i=1}^{K} \Big[\Delta x_i - \mu_j(\Delta x)\Big]^2}, \tag{9}$$

$SD_j(\Delta x)$ was the standard deviation in Δx for the j^{th} patient, K was the total number of rCTs for the j^{th} patient and $i \in [1, K]$; and $SD_j(\Delta y)$ and $SD_j(\Delta z)$ were calculated the same way.

The patient-specific systematic (μ_j) and random (SD_j) errors were then used for determining the standard deviations of systematic errors, Σ_{pop} and standard deviations of random errors, σ_{pop} for the population in all the motion directions. The calculation of Σ_{pop} and σ_{pop} were based on Van Herk's method for determining errors and margins in radiotherapy [Van Herk, 2004], where
The SD of the means per patient were used as an estimator for Σ_{pop};

$$\Sigma_{pop} = \sqrt{\frac{1}{N-1}\sum_{j=1}^{N}\Big[\mu_j(\Delta x) - \mu_{pop}(\Delta x)\Big]^2}, \tag{10}$$

$$\mu_{pop}(\Delta x) = \frac{1}{N}\sum_{j=1}^{N}\mu_j(\Delta x), \tag{11}$$

j is the j^{th} patient of the N patients in the x direction and the same was done for y and z directions. The individual SD_js were used to determine σ_{pop} as the root mean square of $SD_j(\Delta x$);

$$\sigma_{pop} = \sqrt{\frac{1}{N}\sum_{j=1}^{N}\Big[SD_j(\Delta x)\Big]^2}, \tag{12}$$

where j is the j^{th} patient of the N patients and $SD_j(\Delta x)$ is the standard deviation of the j^{th} patient in x direction. The same was done for y and z directions.

5.5.3 Research questions and analysis

(1) How large is interfractional prostate motion relative to bony anatomy?
Interfractional prostate motion occured in Right-Left (x), Posterior-Anterior (y) and Caudal-Cranial (z) directions. Therefore, each of these directional shift gave the magnitude of the shift for every treatment session. This was done by determining μ_j and SD_j for all the three directional motions.

(2) Is there a correlation in motion directions?
Motion in one direction may affect another directional motion. Calculations of correlation coefficients, $\hat{\rho}$ between any two directions (x and y, x and z; and y and z) of motion were done using Equation 13 below (in this formula correlation between x and y);

$$\hat{\rho}_{\Delta x\Delta y} = \frac{S_{\Delta x\Delta y}}{\sqrt{S_{\Delta x\Delta x}S_{\Delta y\Delta y}}} \tag{13}$$

where,

$$S_{\Delta x\Delta x} = \sum(\Delta x)^2 - \frac{(\sum \Delta x)^2}{K_{pop}}\ , \tag{14}$$

$$S_{\Delta y\Delta y} = \sum(\Delta y)^2 - \frac{(\sum \Delta y)^2}{K_{pop}}\ , \tag{15}$$

$$S_{\Delta x\Delta y} = \sum \Delta x\Delta y - \frac{(\sum \Delta x)(\sum \Delta y)}{K_{pop}} \tag{16}$$

and K_{pop} is the total number of rCTs for all the patients. $\hat{\rho}_{\Delta x\Delta z}$ and $\hat{\rho}_{\Delta y\Delta z}$ were calculated the same way.

Scatter plots (x versus y, x versus z and y versus z) were also made and both the calculations and scatter plots helped in ascertaining the correlations between the directions.

(3) What are the proper PTV margins to account for prostate motion when positioning on bony anatomy?
Calculation of the standard deviation of the mean shifts of the population, Σ_{pop} and the root mean square of SD_j, σ_{pop} gave the variables used in the determination of the PTV margins. The direction specific margins; $M_{\Delta x}$, $M_{\Delta y}$ and $M_{\Delta z}$ in the directions x, y and z were then calculated basing on Van Herk formula for errors and margins which works on assumption that 90% of the patient population should receive the minimum dose to the CTV of 95% of the nominal dose (i.e., the dose at the specification point) or higher [Van Herk, 2000]. The margin was calculated as;

$$M = 2.5\Sigma_{pop} + 0.7\sigma_{pop} \tag{17}$$

(4)Which prostate shifts would be appropriate for constructing plan library out of the 3 plans and a conservative plan?
The selection of prostate shifts for construction of a plan library was done basing on the positions of prostate for a shift of +/-1.5SD of the systematic error. The prostate and seminal vesicle positions were chosen basing on directions that had the greatest interfractional motion and directional motion correlations.

5.6 Study B: Comparison of standard treatment with adaptive proton therapy

5.6.1 Aim

To compare standard whole pelvic treatment of high-risk prostate cancer with IMPT to a plan-of-the-day IMPT approach.

5.6.2 Hypothesis

We hypothesize that the treatment approaches give equal minimum dose to the CTVs, but reduced doses (gEUD) to the rectum and bladder with the plan-of-the-day approach.

5.6.3 General-treatment planning

Treatment planning was carried out by the student which involved creating the PTVs by expanding the CTVs. A number of structures were created in both strategies to help in the optimization process and these included PTV50Left, PTV50Right, help volume for PTV50. Other structures created included normal tissues which had a margin of 4cm except 1cm in the cranial-caudal direction around PTV50, cropped 5mm towards PTV50 and PTV60 and also 1.5cm towards the body; rectumout to minimise doses to the rectum and this was cropped 5mm towards PTV60; bladderout to minimise doses to the bladder and was cropped 5mm towards PTV60 and PTV50 and Under67.5 with a margin of 2cm around PTV67.5 to ensure there was no overlap between PTV60 and PTV67.5. After creating all the necessary structures, optimization was done where objectives (Table 5.6.1) were set for helpPTV50, PTV60, PTV67.5, normal tissues, rectum and Under67.5 and dose calculations were then carried out. All prescriptions and doses are given in Gy [RBE], that is, photon dose of 1.1.

Table 5.6.1: Objectives used in optimization.

Structure	Volume [%]	Upper dose [Gy]	Lower dose [Gy]	Priority
PTV50Help	Upper	0.0	51.0	120
	Lower	100.0	49.0	120
PTV60	Upper	0.0	68.0	100
	Upper	36.9	63.4	80
	Lower	100.0	59.0	120
PTV67.5	Upper	0.0	68.5	120
	Lower	100.0	66.5	120
Normal Tissue	Upper	0.0	47.0	100
Rectumout	Upper	0.0	45.0	100
Under67.5	Upper	0.0	61.0	80

No spot smoothing was employed but a spot smoothing radius of 2cm was used. All the structures were created following procedures in Appendix B (Procedure for creating structures in conservative treatment planning) and Appendix C (Procedure for creating structures for plan library treatment planning). The Eclipse treatment planning system (Varian Medical Systems, Palo Alto, USA) was used for generating all IMPT plans and dose re-calculations. All IMPT plans used two lateral opposing fields (90° and 270°) as shown in Figure 14 below.

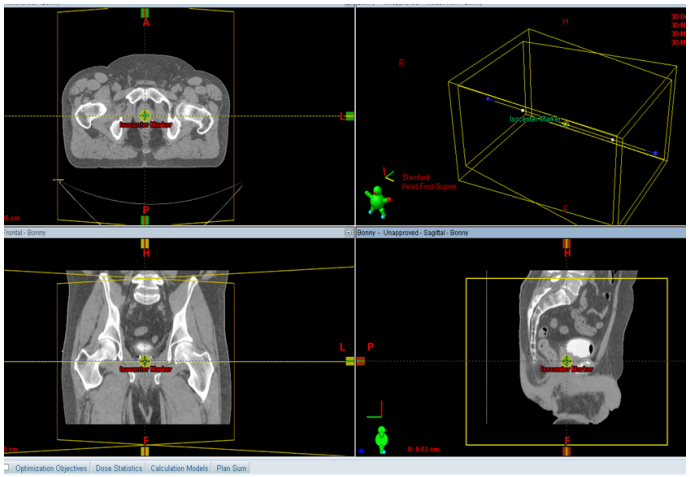

Figure 14: Beam set up for the IMPT (two lateral opposing fields).

5.6.4 Standard treatment

Margins
Results from study A were used to choose margins for the prostate. In the standard treatment planning, an isotropic margin of 5mm [Thörnqvist et al., 2013] was used to create PTV50 around CTV50, a 3mm margin in the left-right and 10mm margins in the cranial-caudal and anterior-posterior and a margin of 5mm in the left-right and 10mm margins in both the cranial-caudal and anterior-posterior were used to create PTV67.5 around CTV67.5 and PTV60 around CTV60 respectively.

Re-calculation of plans on rCTs
The simulation of the proton delivery was done by transferring the plans to each of the rCTs which used rigid registrations based on bony anatomy. The dose distribution for each of the rCT scans was then re-calculated to account for the differences in patient anatomy such as target/organ motion and deformations; and heterogeneities. All these plans were then checked for specified criteria by an independent observer (the supervisor).

5.6.5 Adaptive proton therapy

Margins
A 5mm isotropic margin was used, basing on Thönqvist et al. treatment simulations with a statistical deformable motion model to evaluate margins for multiple targets in radiotherapy for high-risk prostate cancer [Thönqvist S. et al., 2013], for creating PTV67.5, PTV60 and PTV50 while the rest of the other structures were created the same way as in standard/conservative strategy.

Plan library
The plan library for this study was based on three different positions of the PTV67.5 + PTV60 with the position of the lymph node kept constant. Due to correlation in the anterior-posterior (AP) and cranial-caudal (CC) directions (Study A), the library consisted of three (3) PTV67.5 + PTV60-CTVs: 2 PTV67.5 + PTV60-CTVs shifted +/- 1.5 SD of the systematic error in AP (+/- 5.0mm) and CC (+/-4.6mm) direction and 1 PTV67.5 + PTV60-CTV without shift. The positions are as shown in Figures 15 to 18 below.

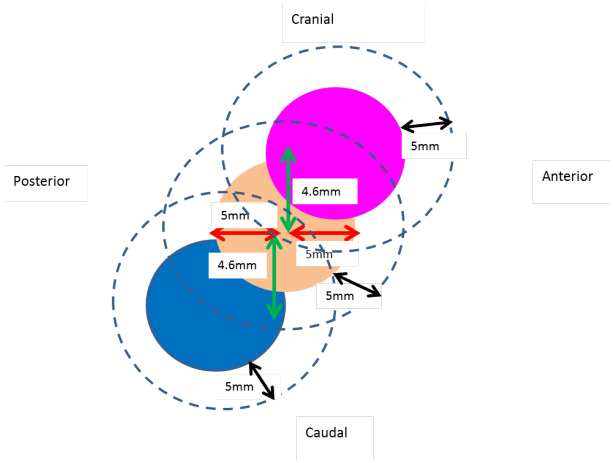

Figure 15: Different positions of the prostate with the corresponding PTVs.

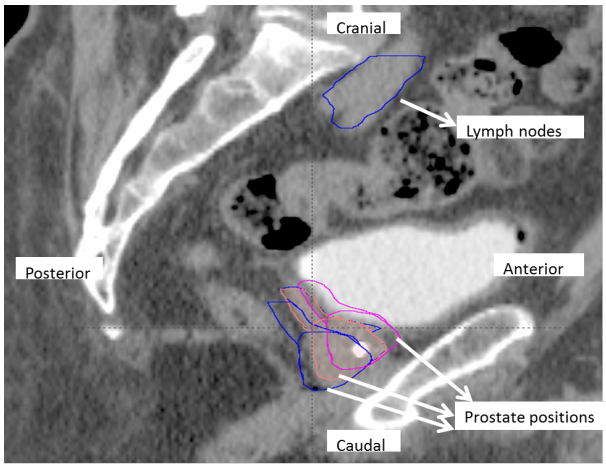

Figure 16: Position of lymph nodes relative to the shifted positions of prostate in CC direction.

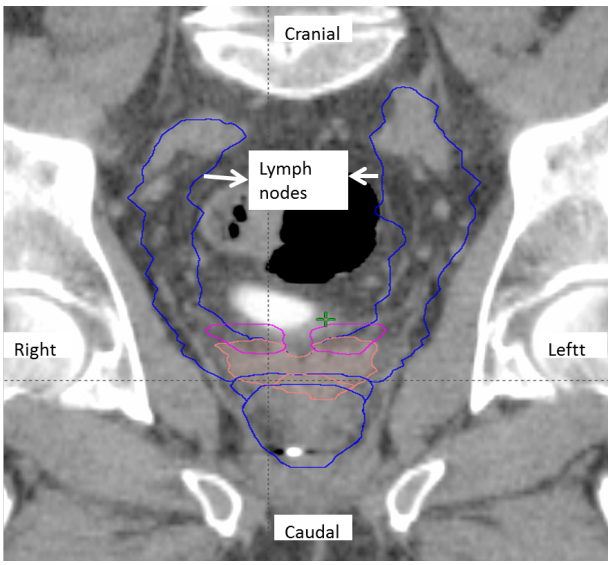

Figure 17: Position of lymph nodes relative to the shifted positions of prostate in RL direction.

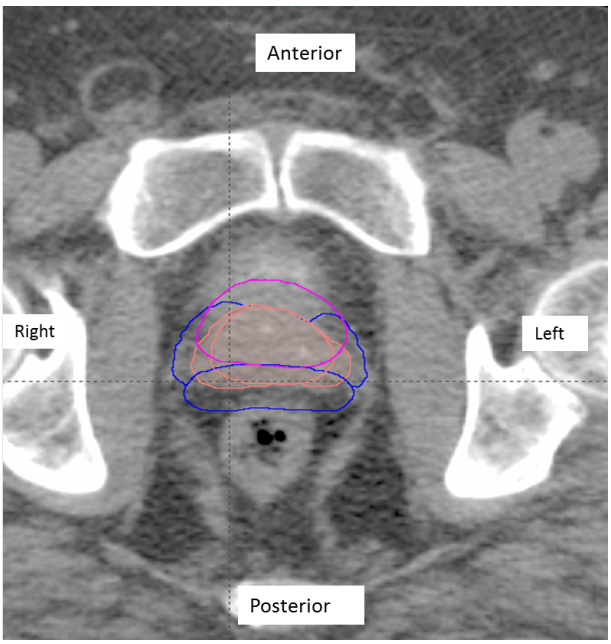

Figure 18: Position of lymph nodes relative to the shifted positions of prostate in AP direction.

For each PTV position, a new treatment plan was created as shown in Table 5.6.2 below.

Table 5.6.2: Plan library selection.

Patient	rCT	Plan selected for PL
1	1	Conservative plan
	2	Conservative plan
	3	Shifted position (-AP, -CC)
	4	No shift
	5	No shift
	6	No shift
	7	No shift
	8	No shift
	9	Shifted position (-AP, -CC)
2	1	Shifted position (+AP, +CC)
	2	No shift
	3	Conservative plan
	4	No shift
	5	No shift
	6	Shifted position (+AP, +CC)
	7	Shifted position (+AP, +CC)
	8	Conservative plan
	9	No shift
3	1	No shift
	2	No shift
	3	Shifted position (+AP, +CC)
	4	Shifted position (+AP, +CC)
	5	Shifted position (+AP, +CC)
	6	No shift
	7	Shifted position (+AP, +CC)
	8	No shift
4	1	Conservative plan
	2	Conservative plan
	3	Conservative plan
	4	Conservative plan
	5	Conservative plan
	6	No shift
	7	Shifted position (-AP, -CC)
	8	Conservative plan
3	1	No shift
	2	Conservative plan
	3	No shift
	4	Conservative plan
	5	Conservative plan
	6	Shifted position (-AP, -CC)
	7	Shifted position (-AP, -CC)
	8	Shifted position (-AP, -CC)
	9	Shifted position (-AP, -CC)

Plan selection and re-calculation of plans

After the plans with prostate in different positions were created, plan selection for the library was then done by the student and verified by the supervisor. These plans were selected by visual

inspection where plans that fit best were evaluated the pCT are chosen according to procedure in appendix D. Bascically, the coverage of rCTV67.5 by the different pPTV67.5 were evaluated.

5.6.6 Variables

For the three targets; CTV67.5, CTV60 and CTV50, $D_{98\%}$ was used to evaluate minimum dose. gEUD for the rectum and bladder were also evaluated. $D_{98\%}$ and the gEUDs were extracted by in-house python script provided by the supervisor. The gEUD for the rectum and bladder were estimated according to Niemierko A. [Niemierko A., 1999] by:

$$EUD = \left(\frac{1}{N} \sum_{i=1}^{N} D_i^k \right)^{\frac{1}{k}} \tag{18}$$

or,
using a differential DVH

$$EUD = \left(\sum_{i=1}^{N} v_i D_i^k \right)^{\frac{1}{k}} \tag{19}$$

where $\{v_i, D_i\}$ are bins of the histogram and "a" is a tissue specific parameter.
In this study, we will use:
k = 12 for rectum,
k = 8 for bladder,
k = 4 for large bowel,
k = 4 for small bowel,
k = 1 is average dose and
k = ∞ is maximum dose.

5.6.7 Analysis

Plots for $D_{98\%}$ for CTV67.5, CTV60 and CTV50 were made for the different treatment sessions for each patient for both the standard and plan library strategies. A t-test was also done between standard and plan library treatment approaches using all rCTs for all the CTVs, rectum, bladder, small and large bowels. These were used to analyze and compare the results of the two treatment strategies that were under investigations.

Chapter 6: Results

6.1 Study A: Prostate target motion relative to bony anatomy

The results of the analysis of study A are presented in the subsequent sections and have been used to answer the research questions.

6.1.1 Interfractional prostate motion

Interfractional prostate motion occured in Right-Left (x), Anterior-Posterior (y) and Caudal-Cranial (z) directions. Histogram and normal distribution approximation curves for these shifts; Δx, Δy and Δz were made as shown in Figures 19 and 20 respwctively below;

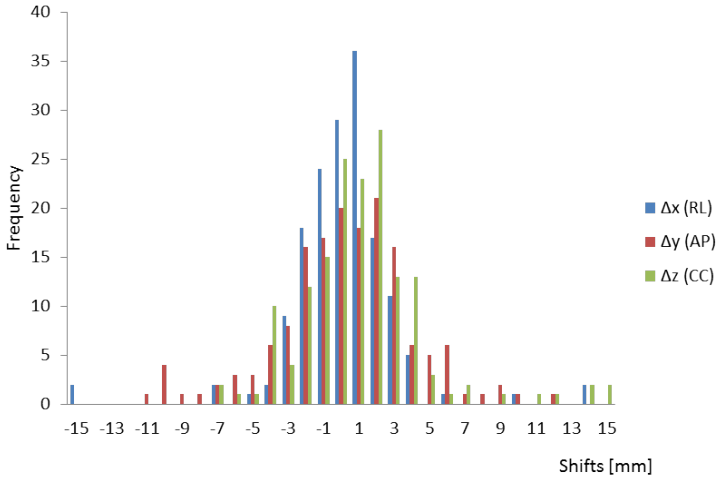

Figure 19: Histogram for shifts in Δx, Δy and Δz.

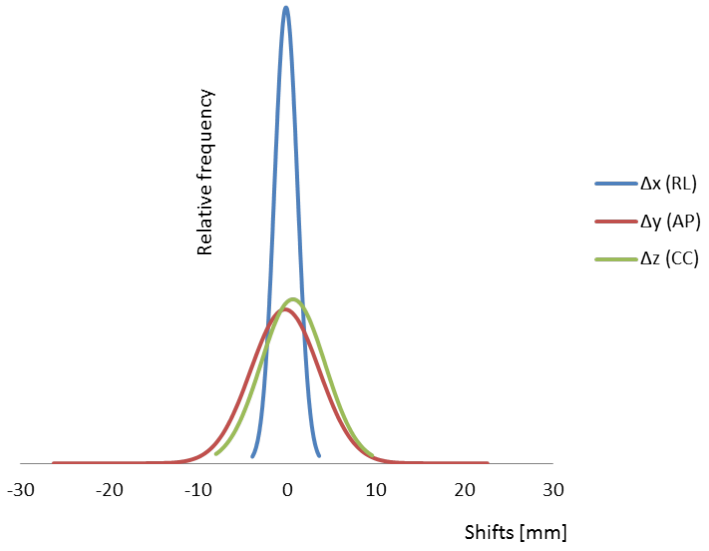

Figure 20: Normal distribution approximation curves in Δx, Δy and Δz.

The above plots for Δx, Δy and Δz showed that these shifts were approximated by normal distributions and that much shift (i.e. prostate motion relative to bony anatomy) occured in AP and CC directions.
A table of estimates for μ_{pop} and Σ_{pop} was as shown in Table 6.1.1 below:

Table 6.1.1: Estimates of μ_{pop} and Σ_{pop}.

Patients, j	$\mu_j(\Delta x)$, (RL) [mm]	$\mu_j(\Delta y)$, (AP) [mm]	$\mu_j(\Delta z)$, (CC) [mm]
1	-1.06	2.36	3.10
2	-0.35	4.97	-4.18
3	0.01	-0.57	0.27
4	1.17	1.16	1.25
5	0.23	-2.65	2.96
6	-0.50	-1.45	2.35
7	0.22	0.52	-0.43
8	-1.22	1.12	0.63
9	-0.36	-4.45	2.23
10	-0.46	-8.56	10.32
11	-0.26	0.22	-1.35
12	1.45	4.82	-0.89
13	-1.56	-0.96	0.92
14	0.61	-2.36	1.01
15	0.18	2.54	-3.41
16	-0.93	2.27	-0.73
17	0.75	-3.10	1.73
18	-0.37	0.79	-1.50
μ_{pop}	**-0.1**	**-0.1**	**0.8**
Σ_{pop}	**0.8**	**3.3**	**3.1**

From table 6.1.1, μ_{pop} were estimated to be -0.1, -0.1 and 0.8 for Δx, Δy and Δz respectivly. The estimated Σ_{pop} were 0.8, 3.3 and 3.1 for Δx, Δy and Δz respectivly.

Histogram and normal distribution approximation curves for systematic errors $\mu_j(\Delta x)$, $\mu_j(\Delta y)$ and $\mu_j(\Delta z)$ were made as shown in Figures 21 and 22 below;

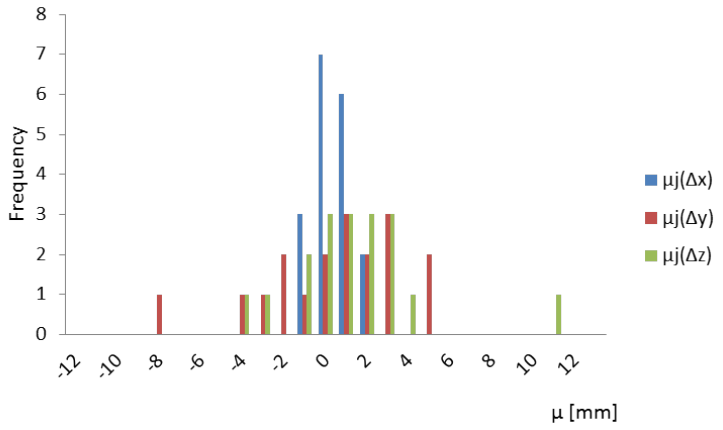

Figure 21: Histogram for $\mu_j(\Delta x)$, $\mu_j(\Delta y)$ and $\mu_j(\Delta z)$.

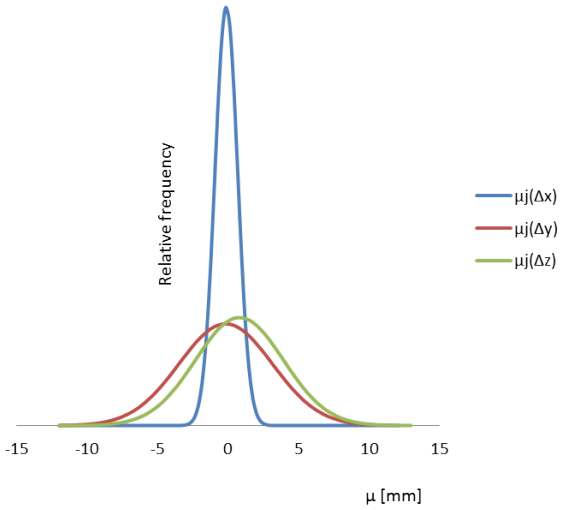

Figure 22: Normal distribution approximation curves for $\mu_j \Delta x$, $\mu_j \Delta y$ and $\mu_j \Delta z$.

A table for $SD_j(\Delta x)$, $SD_j(\Delta y)$ and $SD_j(\Delta z)$, together with σ_{pop} for the population was as shown in Table 6.1.2 below;

Table 6.1.2: Calculated $SD_j(\Delta x)$, $SD_j(\Delta x)$, $SD_j(\Delta z)$ and SD_{pop} for the population.

Patients, j	$SD_j(\Delta x)$ [mm], (RL)	$SD_j(\Delta y)$, (AP) [mm]	$SD_j(\Delta z)$, (CC) [mm]
1	1.39	4.45	1.19
2	0.81	3.34	3.32
3	2.21	1.29	0.93
4	0.84	2.02	1.03
5	1.54	2.90	2.39
6	0.95	2.09	2.37
7	0.91	1.59	1.02
8	0.81	1.38	2.21
9	0.86	1.92	1.61
10	0.98	3.72	4.85
11	0.73	2.72	1.95
12	0.85	2.62	2.44
13	0.87	3.04	2.42
14	1.10	1.64	2.17
15	0.67	0.96	1.88
16	0.88	2.55	0.82
17	1.28	1.98	1.03
18	0.71	1.56	2.51
σ_{pop}	**1.1**	**2.5**	**2.2**

Table 6.1.2 above shows that the estimated σ_{pop} were 1.1, 2.5 and 2.2 for LR, AP and CC respectively.

Both the histogram and normal distribution approximation curves for random errors were also

made as shown in Figures 23 and 24 below;

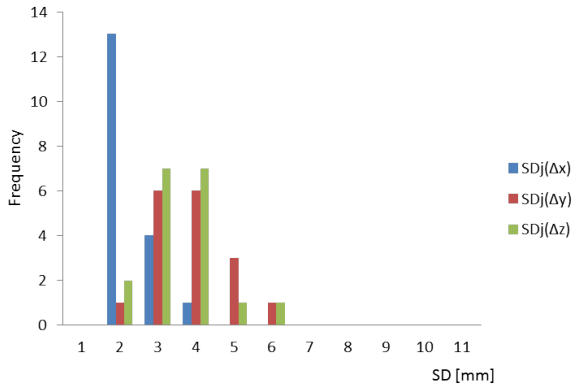

Figure 23: Histogram for $SD_j(\Delta x)$, $SD_j(\Delta y)$ and $SD_j(\Delta z)$.

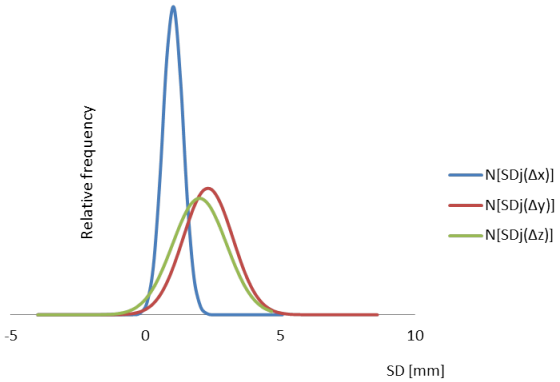

Figure 24: Normal distribution approximation curves for $SD_j(\Delta x)$, $SD_j(\Delta y)$ and $SD_j(\Delta z)$.

6.1.2 Correlation in motion directions

Correlation coefficients between: Δx and Δy, $\hat{\rho}_{\Delta x \Delta y}$ was 0.12; Δx and Δz, $\hat{\rho}_{\Delta x \Delta z}$ was -0.13 and Δy and Δz, $\hat{\rho}_{\Delta y \Delta z}$ was -0.73. This showed clearly that there existed a strong negative linear correlation between y and z where as no linear correlation existed between x and y as well as x and z. Scatter plots for the shifts in the different directions were also made as shown in Figures 25 - 27 below:

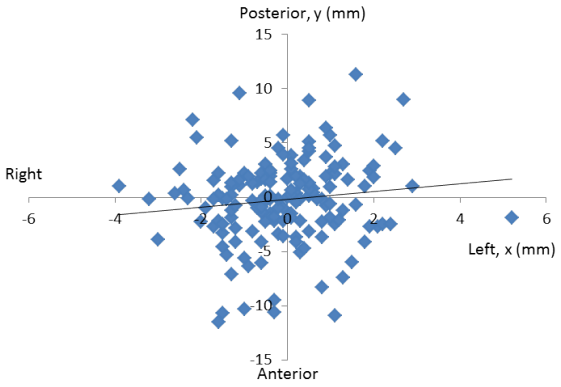

Figure 25: Scatter plot for x against y.

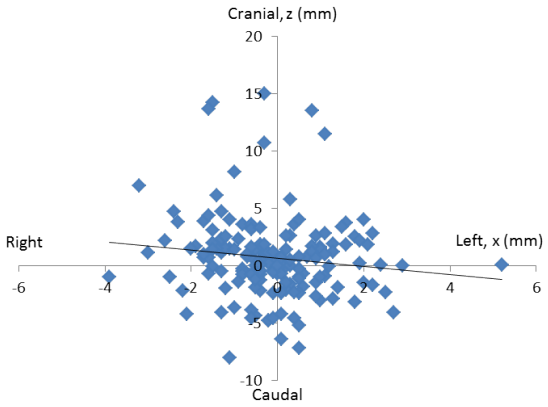

Figure 26: Scatter plot for x against z.

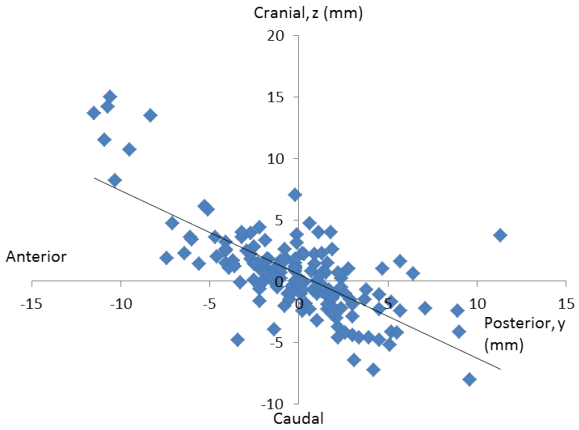

Figure 27: Scatter plot for y against z.

6.1.3 PTV margins to account for prostate motion

Using the Van Herk's margin recipe, the prostate margins when positioned on BA were calculated as:

$$M = 2.5\Sigma_{pop} + 0.7\sigma_{pop} \; in \; mm. \tag{20}$$

$$M_{\Delta x} \approx 2.8 \; mm \tag{21}$$

$$M_{\Delta y} \approx 10.0 \; mm \tag{22}$$

$$M_{\Delta z} \approx 9.4 \; mm, \tag{23}$$

the CTV and its corresponding PTV would look like Figure 28 shown below:

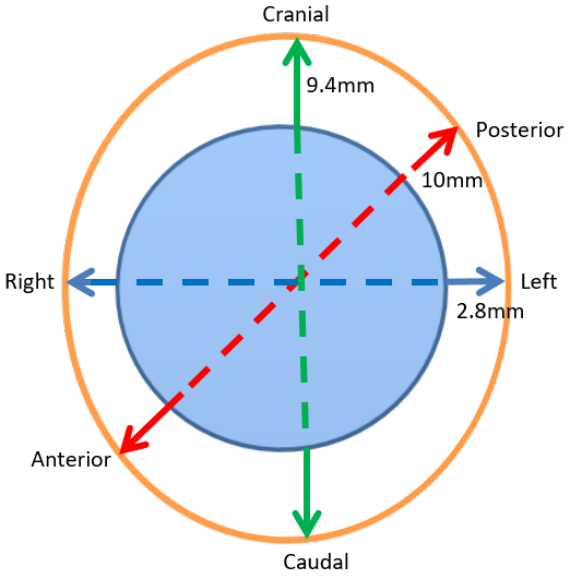

Figure 28: Illustration of PTV and CTV for the margins obtained in Equations 21 - 23.

6.1.4 Appropriate shifts for plan library construction

Three different prostate positions were chosen for this study. Due to correlation in the anterior-posterior (AP) and cranial-caudal (CC) directions, the library consisted of 3 p/sv-CTVs: 2 p/sv-CTVs shifted +/- 1.5 SD of the systematic error in AP (+/- 5.0mm) and CC (+/-4.6mm) direction and 1 p/sv-CTV without shift (Figure 29).

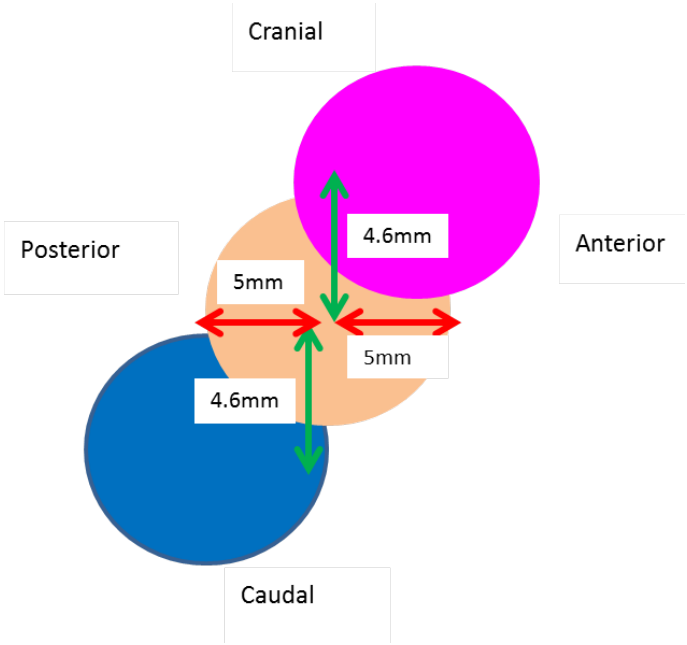

Figure 29: Original prostate position (orange), shifted prostate position 1 (blue) in posterior/caudal direction and shifted prostate position 2 (magenta) in anterior/cranial direction.

6.2 Study B: Comparison of standard treatment with adaptive proton therapy

6.2.1 Comparison of delivered dose to the CTVs

In this study, dose delivery simulation to CTV67.5, CTV60, CTV50, bladder, rectum, small bowel and large bowel were looked at. The simulation of dose delivery to the different CTVs during each session of the treatment for the patients considered for both the standard/conservative and plan library treatments where as shown in Figures 30 - 35 below.

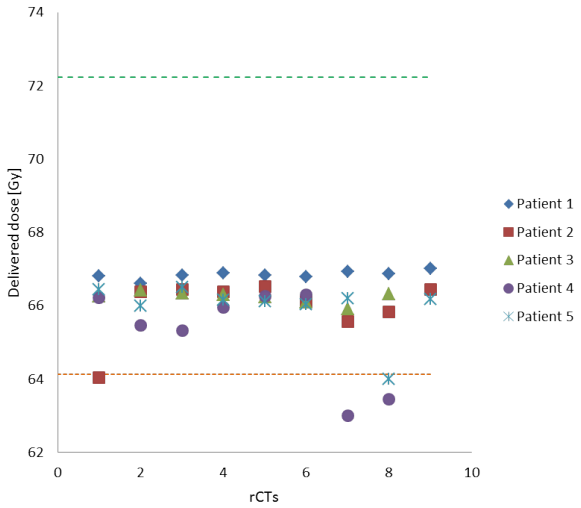

Figure 30: Delivered dose to CTV67.5 for patients in standard treatment strategy on each rCT.

From figure 30, three patients received doses lower than 95% ($D_{98\%}$) of the prescribed dose for at least a treatment session; patient 4 for two treatment sessions while patient 2 and patient 5 for one treatment session each. However, none of the patients received above 107% of the prescribed dose.

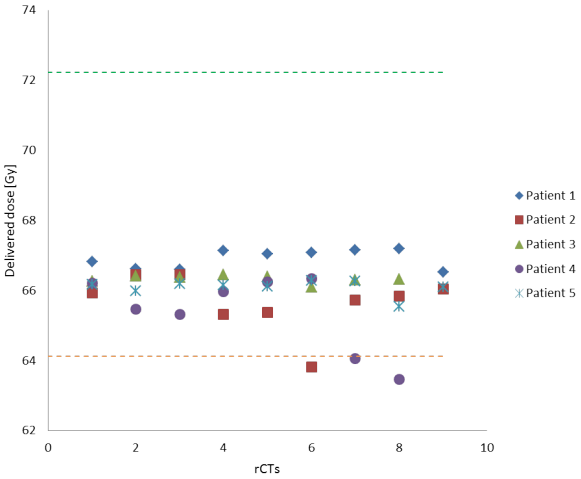

Figure 31: Delivered dose to CTV67.5 for patients in plan library treatment strategy on each rCT.

Figure 31 revealed that two patients received doses lower than 95% ($D_{98\%}$) of the prescribed dose for at least one treatment session with patient 2 for one treatment session and patient 4, two tretament sessions while none received above 107% of the prescribed dose. From statistical analysis (paired t-test) comparing the treatment strategies, it was seen that the mean doses to CTV67.5 for the two strategies were approximately the same; approximately 66.06Gy and 66.08Gy for standard and plan library strategies respectively for p(T $\leq$ t)=0.9.

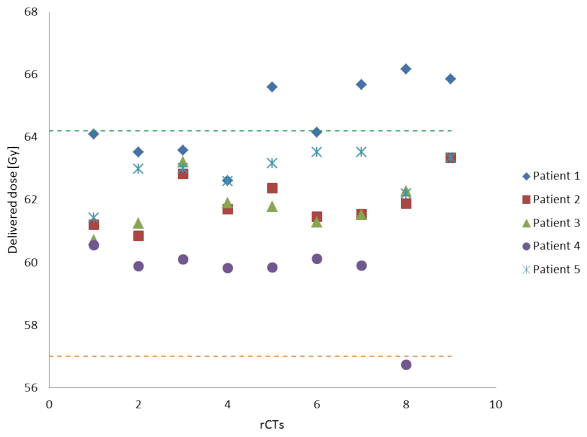

Figure 32: Delivered dose to CTV60 for patients in standard treatment strategy on each rCT.

Figure 32 showed that patient 4 had one tretament session with a dose less than 95% ($D_{98\%}$) of the prescribed dose and patient 1 had four treatment sessions above 107% of the prescribed dose and two treatment sessions with doses just bout 107% of the dose prescribed.

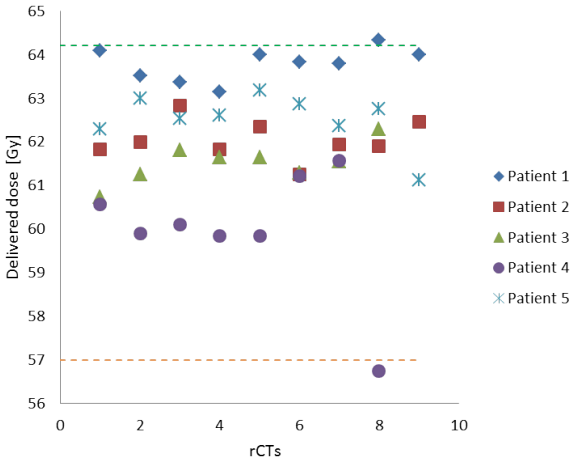

Figure 33: Delivered dose to CTV60 for patients in plan library treatment strategy on each rCT.

Figure 33 showed that patient 1 had one treatment session with higher dose than the maximum prescribed dose of 107% and patient 4 had a lower dose below the 95% ($D_{98\%}$) of the prescribed dose for one session. It was also seen, by statistical analysis (paired t-test), that the mean doses to CTV60 were approximately the same; approximately 62.21Gy and 62.02Gy for standard and plan library strategies respectively $p(T \leq t)=0.1$.

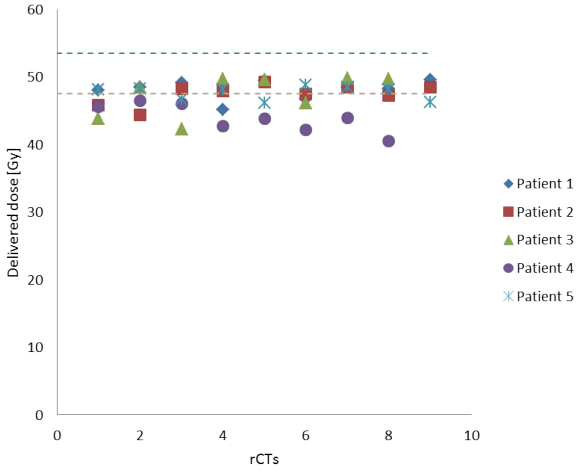

Figure 34: Delivered dose to CTV50 for patients in standard treatment strategy on each rCT.

Figure 34 showed that all patients had at least one treatment session with a dose less than 95% ($D_{98\%}$) of the prescribed dose with two sessions for patient 1, four sessions for patient 2, three sessions for patient 3, all the eight sessions for patient 4 and three sessions for patient 5. However, none of the patients had a dose higher than 100% of the prescribed dose.

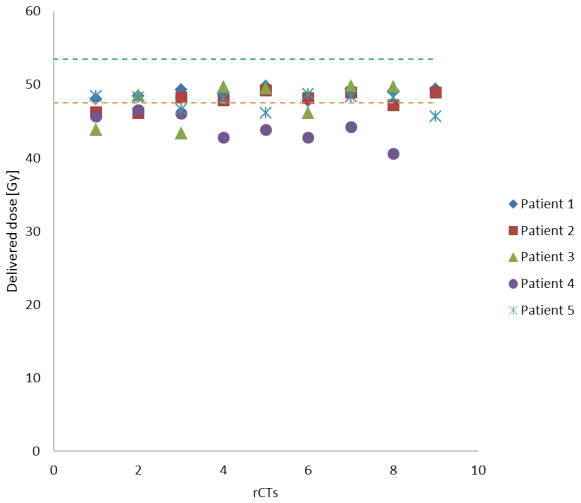

Figure 35: Delivered dose to CTV50 for patients in plan library treatment strategy on each rCT.

Figure 35 showed that all patients had at least one treatment session with a dose less than 95% ($D_{98\%}$) of the prescribed dose with one session for patient 1, three sessions for patient 2, three sessions for patient 3, all the eight sessions for patient 4 and three sessions for patient 5 while none of the patients had a dose higher than 100% of the prescribed dose. Statistical analysis (paired t-test) revealed that the mean doses to CTV50 were approximately 46.98Gy and 47,25Gy for standard and plan library strategies respectively. The mean doses to CTV50 for both strategies were approximately the same but a much better dose coverage was achieved with plan library.

6.2.2 Comparison of delivered doses to OARs

The results showed a reduction in the mean dose of approximately 3.1Gy gEUD for rectum (k=12) with p(T $\leq$ t)=0.00004 and approximately 1.9Gy gEUD for bladder (k=8) with p(T $\leq$ t)=0.00009 using plan library strategy while the mean dose to the large and small bowels were approximately the same for the two approaches. Mean gEUDs were approximately 29.7Gy and 29.8Gy with p(T $\leq$ t)=0.7 for large bowels (k=4) for standard and plan library approaches respectively while the mean gEUDs for the small bowels (k=4) were approximately 24.44Gy and 24.41Gy with p(T $\leq$ t)=0.5 for standard and plan library strategies respectively.

Chapter 7: Discussion and Conclusion

7.1 Discussion

In this master project we have estimated in a patient-population how prostate move in relation to bony anatomy and used this to construct a plan library for use in proton therapy of high-risk prostate cancer patients who simultaneously receive treatment to the prostate, seminal vesicles and pelvic lymph nodes (study A). This plan library approach was also shown to be feasible in a simulation study of five independent high-risk prostate cancer patients (Study B). Compared to standard proton therapy, the plan library approach resulted in reduced estimated treatment doses (gEUD) to the rectum and bladder while maintaining similar estimated treatment minimum doses to the CTVs.

To our knowledge this is the first project investigating the use of a population-based plan library in proton therapy of high-risk prostate cancer patients. Another study was conducted where a patient-specific library of PTV was used in plan-of-the day adaptation for interfractional motion mitigation [Wenjing C. et al., 2013]. Multiple images taken on different days were used with delineations of both the target and OARs to create the plan library which was then used for treatment. This method was tested for feasibility and effectiveness in a retrospective tretament-planning which resulted into satisfactory target coverage with a slightly increased delivered dose to the OARs [Wenjing C. et al., 2013]. Yet another study carried out on prostate cancer treatment using proton therapy involved online adaptive procedure to mitigate the effect of prostate motion relative to bony anatomy and was compared to non- adaptive procedure [Zhang M. et al., 2011]. It was established that the non-adaptive method resulted into a degradation in the delivered dose while the adaptive procedure was effective depending on whether the technique used was two-field opposing spot 3D-modulation or 24-field full arc distal edge tracking (DET) [Zhang M. et al., 2011]. This study found out that the 3D-modulation was more robust than DET [Zhang M. et al., 2011]. The reason was due to the number of beam angles with DET having more beam angles and hence for any direction of prostate shift, there were always beams perpendicular to motion direction leading to high doses [Zhang M. et al., 2011]. Compared to these methods, our method is simpler as it requires only a single pCT for plan library generation and plan selection could be performed without target delineation.

In our study, study A, from a population of 18 patients, it was established that there were motion of prostate in all directions relative to bony anatomy. Greatest motion took place in the AP and CC directions and least in the RL direction. This motion could have been due to a number of sources, but no specific cause was identified in the study. A number of studies have been carried out, compiled and reviewed regarding organ motion and its management [Langen K.M. et al., 2001]. These studies ranges from position-related organ motion to interfractional organ motion. It was seen from the different studies that there was no single specific value of motion but rather a range of values, and all these were within the same range [Langen K.M. et al., 2001]. These studies confirm our findings, that is; there is less motion in the RL direction compared to AP and CC directions and that our values were in the range prescribed by other authors. Chris B. et al. did a study to determine the target volume PTV margins for prostate [Chris B. et al., 2008]. Here the prostate position was localized using implanted gold seeds in the prostate with respect to the bony anatomy and margins determined to find the degree of motion [Chris B. et al., 2008]. They found that the BA localization leads to a setup margin of 3.1mm, 8.9mm and 10.7mm in the LR, IS and AP directions respectively, and that Σ were 0.9mm, 3.0mm and 3.5mm while σ were 1.2mm, 2.0mm and 2.8mm in the LR, IS and AP directions respectively. These values were similar to our findings. Furthermore, our study revealed that there existed a strong negative linear correlation between two motion directions; AP and CC as was demonstrated in the scatter plot (Figure 27). This literally meant there was simultaneous motion in the AP and CC direction which could affect treatment. To mitigate this motion challenge, we constructed a plan library with prostate in three different positions as well as one position where the prostate was not shifted except larger margins were used. A challenge with the feasibility of a plan library approach is the manual selection of treatment plans which limits the number of plans included in the plan library. In this study we limited the number of plans to four (4). This was possible by exploiting the correlation of motion in the anterior-superior direction and inferior-posterior direction established in study A. Study B showed similar trends in the dose distributions uisng both the standard and plan library strategies in terms of dose distributions to CTV67.5, CTV60 and CTV50. However, the trend in dose distribution in CTV50 showed missing of the targets in most of the treatment sessions by almost all the patients who were being used for the study for both strategies. This could have been attributed to the delineation errors, errors due to skin motion with respect to internal

anatomy, imaging errors due to arbitrary position of prostate or interference of the scanning process and organ and setup errors. There was reduced doses to the rectum and the bladder using the plan library approach while the gEUD to the small and large bowels showed no much difference. The method of plan library proved to be a simple feasible method since you do not need target delineation each time you should carry out a treatment in a given treatment session. However, it is more cumbersome compared to the standard treatment approach.

7.2 Conclusion

Uncertainties such as setup errors and organ motions are inevitable during proton therapy just like in any other radiotherapy technique although this treatment option has proven to be effective. This therefore means measures have to be put in place to ensure treatment is carried out in the best way possible. One of the ways we tried to investigate in this master project was to determine the degree of interfractional prostate motion relative to the bony anatomy and shift the prostate accordingly. This investigation was based on a population of patients to help determine margins that were used to create the PTVs and to construct a plan library. This plan library construction aimed at establishing the doses delivered to the targets compared to the standard approach as well as comparing the gEUD to the rectum and bladder with respect to the standard approach.

This approach indeed resulted in reduced estimated treatment doses (gEUD) to the rectum and bladder while there was a comparable estimated treatment minimum doses to the CTVs as well as the small and large bowels. The plan library approach based on a population information about prostate motion relative to bony anatomy thus proved to be feasible.

References

[1] Albert J. et al (2014). "High-Risk" Prostate Cancer: Classification and Therapy. Nature Reviews Clinical Oncology 11, pp:308-323.

[2] Albin F., Anders F. and Bjorn H. (2011). Minimax optimization for handling range and setup uncertainties in proton therapy. Medical Physics ;doi:10.1118/1.3556559.

[3] Alex T. (1994). Module 13: Treatment volumes and treatment planning in proton therapy. www.oncolink.org.pp:6.

[4] Alexei T., Paul L., Jason A. et al. (2011). Interfractional variations in the setup of pelvic bony anatomy and soft tissue, and their implications on the delivery of proton therapy for localized prostate cancer. Int J Radiat Oncol Biol Phys ;80 pp:928-937.

[5] Amaldi U. and Kraft G.(2005). Radiotherapy with beams of carbon ions. Reports on Progress in Physics 68.8 , pp:1861-1882.

[6] Andreo P. (2009). On the clinical spatial resolution achievable with protons and heavier charged particle radiotherapy beams. Physics in Medicine and Biology 54.11 , N205-N215.

[7] Ayal A.A. et al. (2009). Whole pelvic radiotherapy versus prostate only radiotherapy in the management of locally advanced or aggressive prostate; Int. J. Radiation Oncology Biol. Phys., Vol. 75, No. 5, pp:13441349.

[8] Borges H. L., Linden R. and Wang J. Y. (2008). DNA damage-induced cell death. Cell research 18.1 , pp: 17-26.

[9] Brenner D.J. (1999), Hall E.J. Fractionation and protraction for radiotherapy of prostate carcinoma. Int J Radiat Oncol Biol Phys. ;43:1095101.

[10] Carolyn V, (2015). Proton Therapy: Behind the Scenes, The Abramson Cancer Center of the University of Pennsylvania.

[11] Cember H. and Johnson T. (2008). Introduction to Health Physics. 4^{th} ed. McGraw-Hill Education/Medical.

[12] Chris B. et al. (2008). Planning target margin clculations for prostate radiotherapy based on intrafraction and interfraction motion using four localization methods. Int. J. Radiation Oncology Biol. Phys, Vol. 70, No. 1 , pp. 289-298.

[13] Clark V. H. et al. (2008). IMRT treatment planning for prostate cancer using prioritized prescription optimization and mean-tail-dose functions. Linear Algebra Appl. ; 428(5-6) pp:1345-1364.

[14] Cotrutz C., Lahanas M., Kappas C., Baltas D. (2001). A multi objective gradient-based dose optimization algorithm for external beam conformal radiotherapy. Phys Med Biol;46 pp: 216175.

[15] Craft D., Halabi T., Bortfeld T. (2005). Exploration of trade offs in intensity-modulated radiotherapy. Phys Med Biol;50 pp:585768.

[16] Craig E. et al. (2004). Implementing IMRT in clinical practice: a joint document of the American Society for Therapeutic Radiology and Oncology and the American Association of Physicists in Medicine. International Journal of Radiation Oncology*Biology*Physics Volume 58, Issue 5, pp:1616-1634.

[17] Cristen B. (2013), The promise of proton therapy, Applied radiation Oncology, pp:37.

[18] D'Amico et al. (2002). Biochemical outcome after radical prostatectomy or external beam radiation therapy for patients with clinically localized prostate carcinoma in the prostate specific antigen era. American Cancer Society;95 pp:2816.

[19] Dau A. (2007). Is the / Value for Prostate Tumours Low Enough to be Safely Used in Clinical Trials? Clinical Oncology, 19:289301.

[20] Dawson L.A. and Jaffray D.A. (2007). Advances in image-guided radiation therapy. J. Clin. Oncol.;25:93846.

[21] Dr. James E. Parks. The Compton Effect-Compton Scattering and Gamma Ray Spectroscopy. pp:18.

[22] Engelsman M., Schwarz M. and Dong L. (2013). Physics Controversies in Proton Therapy. Seminars in Radiation Oncology 23.2, pp. 88-96.

[23] Erminia I. (2015). Clinical utility of RapidArcTM radiotherapy technology Cancer Management and Research :7 345356.

[24] Fowler J.F. (2010). 21 years of biologically effective dose. Br J Radiol, 83:554568.

[25] Grupen C. and Buvat I. (2011). Handbook of Particle Detection and Imaging.2012^{th} ed. Springer.

[26] Gupta T. and Anand C.N. (2012). Image-guided radiation therapy: Physician's perspectives, Journal of Medical Physics/Association of Medical Physicists of India, 2012 Oct-Dec; 37(4): 174182.

[27] Hall E. J. and Giaccia A. J. (2011). Radiobiology for the Radiologist. Seventh, Lippincott Williams and Wilkins.

[28] Hoppe B., Henderson R. and Mendenhall W.M. (2011). Proton therapy for prostate cancer. Oncology. 25:644-650.

[29] Hui L. and Chang J.Y. (2011). Proton therapy in clinical practice. Chin J Cancer; 30(5): 315326.doi: 10.5732/cjc.010.10529.

[30] ICRP (1977). ICRP Publication 26: Recommendations of the ICRP. 1^{st} ed. SAGE Publications Ltd.

[31] ICRU Report 83 (2010). Prescribing, Recording, and Reporting Photon-Beam Intensity-Modulated Radiation Therapy (IMRT), Journal of the ICRU, Volume 10 No.1, pp:13 -53.

[32] ICRP (2013). ICRP Publication 103: Recommendations of the ICRP. 1^{st} ed. SAGE Publications Ltd.

[33] ICRU Report 78 (2009). Prescribing, Recording, and Reporting Proton- Beam Therapy. International Journal of Radiation Oncology * Biology * Physics 73.5, p.1602.

[34] Indra J.Das and Harald Paganetti ("n.d"). Introduction and History of Proton Therapy, Department of Radiation Oncology, Indiana University School of Medicine Indianapolis, IN and Department of Radiation Oncology, Massachusetts General Hospital and Harvard Medical School Boston, MA: pp. 5.

[35] James A.P. (1999). 3D Treatment Planning and Intensity-Modulated Radiation Therapy. Oncol. Review Article October 01, 1999.

[36] James M. METZ (2010). Proton Therapy, Demos Medical, Radiation Medicine Rounds, vol. I, Issue 3, New York.

[37] Jared H. Quantum Physics. Beginner's guide to amazing Physics theories, 2^{nd} Ed., pp. 33.

[38] Jie Y., Pengcheng Z., Liyuan Z., Huazhong S., Baosheng L. and Zhiguo G. (2017). Particle swarm optimizer for weighting factor selection in intensity modulated radiation therapy optimization algorithms. Physica Medica 33, pp:136-145.

[39] Kaderka R. (2011). Out-of-field dose measurements in radiotherapy. PhD thesis. Technische Universitat Darmstadt.

[40] Kelley M. R (2011). DNA Repair in Cancer Therapy: Molecular Targets and Clinical Applications. 1^{st} ed. Academic Press. Retrieved from: https://www.elsevier.com/books/dna-repair-in-cancer-therapy/kelley/978-0-12-384999-1.

[41] Langen K.M. et al. (2001). Organ moton and itsmanagement.Int. J. Radiation OncologyBiol. Phys., Vol.50, No.1,pp:265-278.

[42] Lederman M. (1981). The early history of radiotherapy: 1895-1934. International Journal of Radiation Oncology * Biology * Physics 7.5, pp: 639-648.

[43] Leo W. R. (1994). Techniques for Nuclear and Particle Physics Experiments. 2^{nd} Rev. Springer.

[44] Linus C.B., Alison C.T. and David P.D. (2017). The Role of Hypofractionated Radiotherapy in Prostate Cancer. Curr Oncol Rep 19: 30.

[45] Linz U. (2011). Ion Beam Therapy: Fundamentals, Technology, Clinical Applications (Biological and Medical Physics, Biomedical Engineering). 2012^{th} ed. Springer.

[46] Lomax A.J. (2008). Intensity-modulated proton therapy and its sensitivity to treatment uncertainties 1: the potential effects of calculational uncertainties. Phys. Med. Biol.;53:1027-1042.

[47] Ludvid P M. (2013), Establishing and expanding the indications for proton and particle therapy, Acta Oncol.;52(3) pp:459-62..

[48] Marcel V. H. (2004), Seminars in Radiation Oncology, Vol 14, No 1 (January) : pp 52-64.

[49] Martijn E., Marco S., and Lei D. (2013). Physics Controversies in Proton Therapy, Semin Radiat Oncol 23:88-96.

[50] Martin J. (2016). Particle Therapy Patient Statistics (per end of 2015). Copyright @ PTCOG.

[51] Mayles P., Nahum A. and Rosenwald J. C. (2007). Handbook of Radiotherapy Physics: Theory and Practice. 1^{st} ed. CRC Press.

[52] Michel G., Yan D. and Alvaro M. (2010). Adaptive Radiation Therapy for Prostate Cancer, Seminars in radiation oncology.;20(2):130-137.

[53] Miralbell R., Roberts S.A., Zubizarreta E. and Hendry J.H. (2012). Dose-Fractionation Sensitivity of Prostate Cancer Deduced From Radiotherapy Outcomes of 5,969 Patients in Seven International Institutional Datasets. Int J Rad Oncol Biol Physics, 82:e17e24.

[54] Mottet N. (2015), Guidelines on Prostate Cancer, European Association of Urology: pp 17.

[55] Nam P.N., Rick D., Satya R.Bose et al. (2015). Potential Applications of Image-Guided Radiotherapy for Radiation Dose Escalation in Patients with Early Stage High-Risk Prostate Cancer.Front Oncol. ; 5: 18.

[56] National Association for Proton Therapy Website.http://www.proton-therapy.org/facts.htm. Accessed September 15, 2010.

[57] Nicolas M. et al. (2017). EAU-ESTRO-SIOG Guidelines on Prostate Cancer. Part 1: Screening, Diagnosis, and Local Treatment with Curative Intent; Volume 71, Issue 4, April, pp: 618-629.

[58] Niemierko A. A. (1999). Generalized concept of equivalent uniform dose (EUD) Med Phys. ;26:1100.

[59] Olive K. A. and Particle Data Group (2014). Review of Particle Physics. Chinese Physics C 38.9, p.090001.

[60] OSullivan B., Wunder J. and Pisters P.W.T. (2004). Clinical Target Volumes in Conformal and Intensity Modulated Radiation Therapy. A clinical guide to cancer treatment, Springer,pp:206-208.

[61] Paganetti H. et al. (2002). Relative biological effectiveness (RBE) values for proton beam therapy. International Journal of Radiation Oncology * Biology * Physics 53.2 , pp: 407-472.

[62] Paganetti H. (2011). Proton Therapy Physics (Series in Medical Physics and Biomedical Engineering). 1^{st} ed. CRC Press.

[63] Paganetti H. (2012). Range uncertainties in proton therapy and the role of Monte Carlo simulations. Physics in Medicine and Biology 57.11, R99-R117.

[64] Paganetti H. (2015). Relating Proton Treatments to Photon Treatments via the Relative Biological Effectiveness-Should We Revise Current Clinical Practice? International Journal of Radiation Oncology * Biology * Physics 91.5 , pp: 892-894.

[65] Piet D., Karin H., Sara J., Rodney W., Raymond O., Hendrik VP. (2006). The role of whole pelvic radiotherapy in locally advanced prostate cancer, Radiotherapy and Oncology 79 (2006) 114: pp 2,3.

[66] Pugh T.J. and Lee A.K. (2014). Proton beam therapy for the treatment of prostate cancer; Cancer J. Nov-Dec;20(6):415-20.

[67] Rajamanickam B. et al. (2014). Biological response of cancer cells to radiation treatment. Front. Mol. Biosci. Volume 1, Article 24, pp:3.

[68] Reco C, Clifton Ling C. (2008). Broadening the scope of image-guided radiotherapy (IGRT) Acta Oncol. ;47:1193200.

[69] Roach M., DeSilvio M. and Lawton C. (2003). Phase III trial comparing whole-pelvic versus prostate-only radiotherapy and neoadjuvant versus adjuvant combined androgen suppression: Radiation Therapy Oncology Group 9413. J Clin Oncol;21:1904 1911.

[70] Saha G. B. (2006). Physics and Radiobiology of Nuclear Medicine. 3rd. Springer.

[71] Schippers J. M. (2009). Beam delivery systems for particle radiation therapy: current status and recent developments. Reviews of Accelerator Science and Technology 2.01 , pp: 179-200.

[72] Schlegel W. C. et al. (2006). New Technologies in Radiation Oncology (MedicalRadiology). 2006^{th}ed. Springer.

[73] Schulz-Ertner D., Jakel O. and Schlegel W.(2006). Radiation Therapy With Charged Particles. Seminars in Radiation Oncology 16.4 , pp: 249-259.

[74] Sejpal S.V., Amos R.A., Bluett J.B. et al. (2009). Dosimetric changes resulting from patient rotational setup errors in proton therapy prostate plans. Int. J. Radiat. Oncol. Biol. Phys. ;75:40-48.

[75] Sengbusch E. et al. (2009). Maximum proton kinetic energy and patient - generated neutron fuence considerations in proton beam arc delivery radiation therapy.Medical Physics 36.2 , pp. 364-372.

[76] Shinohara E. (2016). An introduction to proton therapy. The Abramson Cancer Center of the University of Pennsylvania, OncoLink , pp. 1-4.

[77] Stephanie L. and Riesterer O. (2013). Modern Techniques in Radiation Oncology. Retrieved frohttp://www.sps.ch/fr/articles/progresses/modern-techniques-in-radiation-oncology-36/.

[78] Stroom J.C.et al. (1999). Inclusion of geometrical uncertainties in radiotherapy treatment planning by means of coverage probability. Int. J. Radiat. Oncol. Biol. Phys. ;43:905919.

[79] Stroom J.C. et al. (2002). Geometrical uncertainties, radiotherapy planning margins, and the ICRU-62 report. Radiotherapy and Oncology 64, pp:7583.

[80] Thariat J. et al. (2012). Past, present, and future of radiotherapy for the benefit of patients.Nature Reviews Clinical Oncology 10.1 , pp. 52-60.

[81] Thieke C., Kufer K., Monz M., Scherrer A., Alonso F., Oelfke U., et al. A new concept for interactive radiotherapy planning with multicriteria optimization: first clinical evaluation. Radiother Oncol 2007;85:2928.

[82] Thomas D. J. (2012). ICRU Report 85, Fundamental Quantities and Units for Ionizing Radiation. Radiation Protection Dosimetry 150.4 , pp. 550-552. issn: 0144-8420, 1742-3406.

[83] Thönqvist S. et al. (2013). Degradation of target coverage due to inter-fraction motion during intensity-modulated proton therapy of prostate and elective targets. Acta Oncol. Apr;52(3):521-7.

[84] Thönqvist et al. (2013). Treatment simulations with a statistical deformable motion model to evaluate margins for multiple targets in radiotherapy for high-risk prostate cancer. Radio. Oncol. Dec;109(3):344-9.

[85] Timlin, C. and Jones, B. (2010), Proton and Charged Particle Radiotherapy, The British Journal of Radiology, 83, 87.

[86] Trofimov A., Nguyen P.L., Coen J.J et al. (2007). Radiotherapy treatment of early-stage prostate cancer with IMRT and protons: a treatment planning study. Int J Radiat Oncol Biol Phys;69, pp:444-453.

[87] Van Kranen S. et al. (2009). Setup uncertainties of anatomical sub-regions in head-and-neck cancer patients after offline CBCT guidance. Int J Radiat Oncol Biol Phys ;73:1566-1573.

[88] Verellen D, Ridder MD, Storme G. A. (2008). (Short) history of image-guided radiotherapy. Radiother Oncol. ;86, pp:413.

[89] WilsonR. R. (1946). Radiological use of fast protons.Radiology 47.5 , pp. 487-491.

[90] www.oncolink.org, Trustees of The University of Pennsylvania, 2016.

[91] Xia P. et al. (2010). Comparison of three strategies in management of independent movement of the prostate and pelvic lymph nodes. Med Phys. Sep;37(9):5006-13.

[92] Yoon M., Kim D., Shin D.H. et al. (2008). Inter- and intrafractional movement-induced dose reduction of prostate target volume in proton beam treatment. Int J Radiat Oncol Biol Phys ;71:1091-1102.

[93] Zelefsky M.J.et al. (2002). High-dose intensity modulated radiation therapy for prostate cancer: early toxicity and biochemical outcome in 772 patients. Int J Radiat Oncol Biol Phys. ;53:11116.

[94] Zhang X., Dong L., Lee A.K. et al. (2007). Effect of anatomic motion on proton therapy dose distributions in prostate cancer treatment. Int J Radiat Oncol Biol Phys ;67:620-629.

[95] Ziegler J. F. (1999). Stopping of energetic light ions in elemental matter. Journal of Applied Physics 85.3 , pp. 1249-1272.

[96] Zietman A., Bae K., Slater J.D., Shipley W.U., Efstathiou J.A. and Coen J.J. (2009). Randomized trial comparing conventional-dose with high-dose conformal radiation therapy in early-stage adenocarcinoma of the prostate: long-term results from proton radiation oncology group/American College of Radiology 95-09. J. Clin. Oncol. 28:110611.10.1200/JCO.25.8475.

[97] Zietman A., Moughan J., Owen J.and Hanks G. (2001). The Patterns of Care Survey of radiation therapy in localized prostate cancer: similarities between the practice nationally and in minority-rich areas. Int. J. Radiat. Oncol. Biol. Phys. ;50:7580.

APPENDIX A
Procedure for registration

a) When you login to the Eclipse TPS; you go to quicklinks, choose imaging and then image registration and finally click ok.

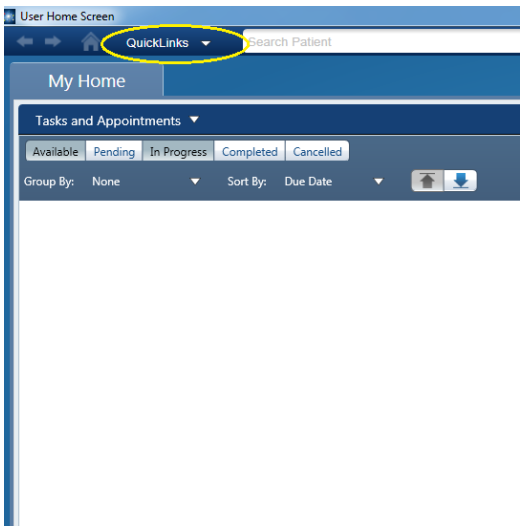

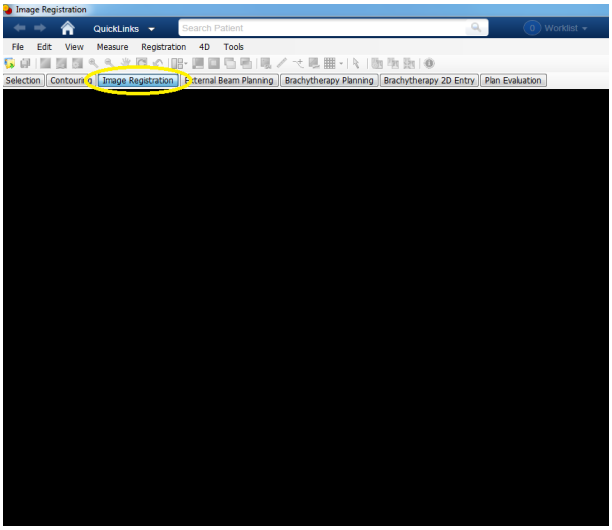

b) In the top dialogue box, you then search for the patient you want to do registration on, in this case zzprostHUH23.

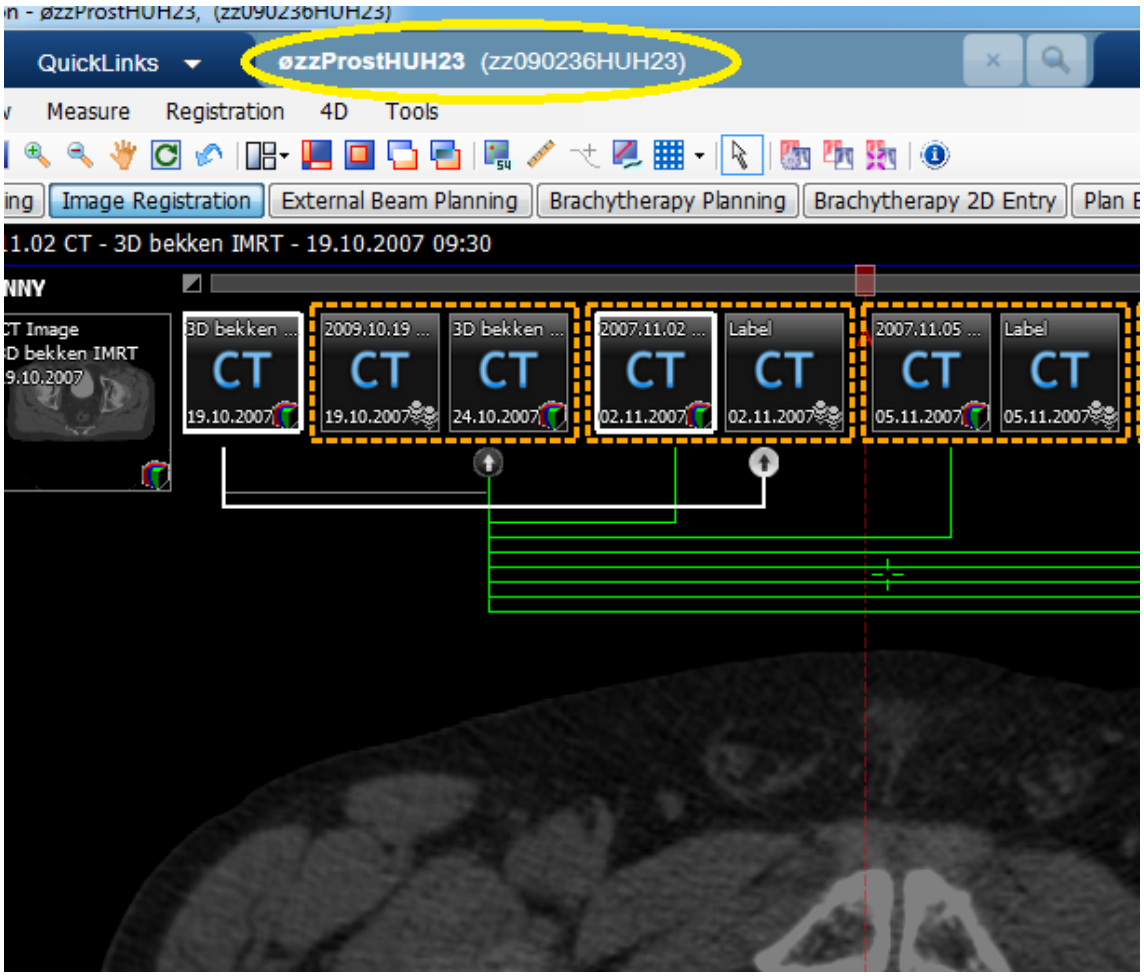

c) You then go to the rCT you want to do registration and double click to open.

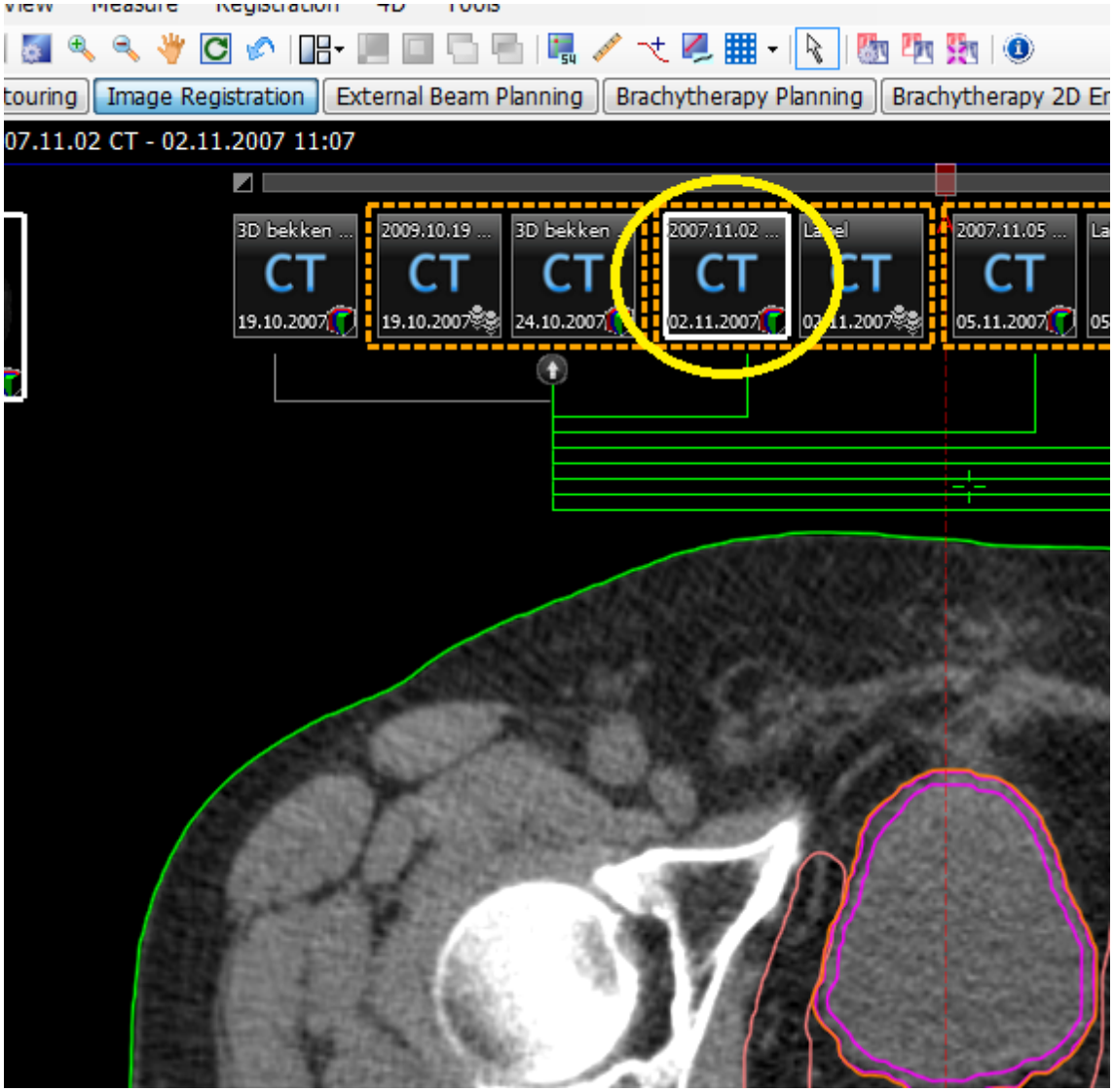

d) Click registration and choose automatic matching.

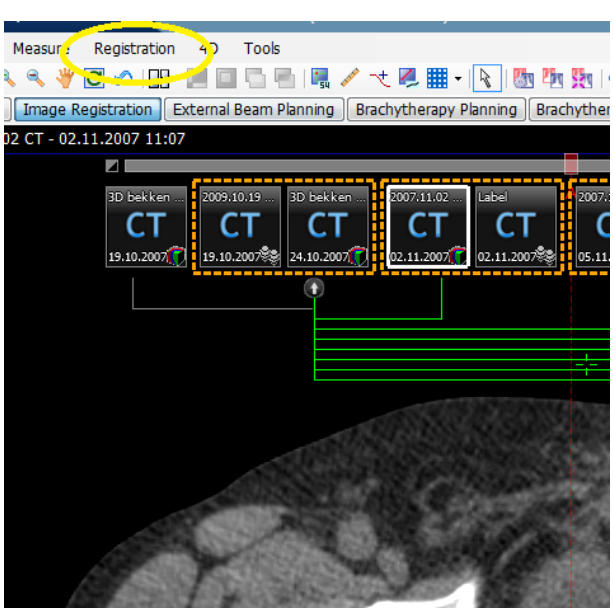

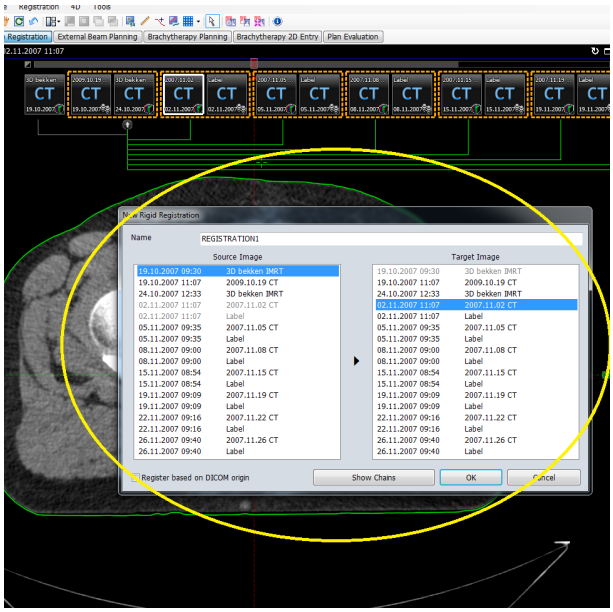

e) Rename the registration e.g BONNY and then select the source image which is the pCT as well as the rCT which is the target.

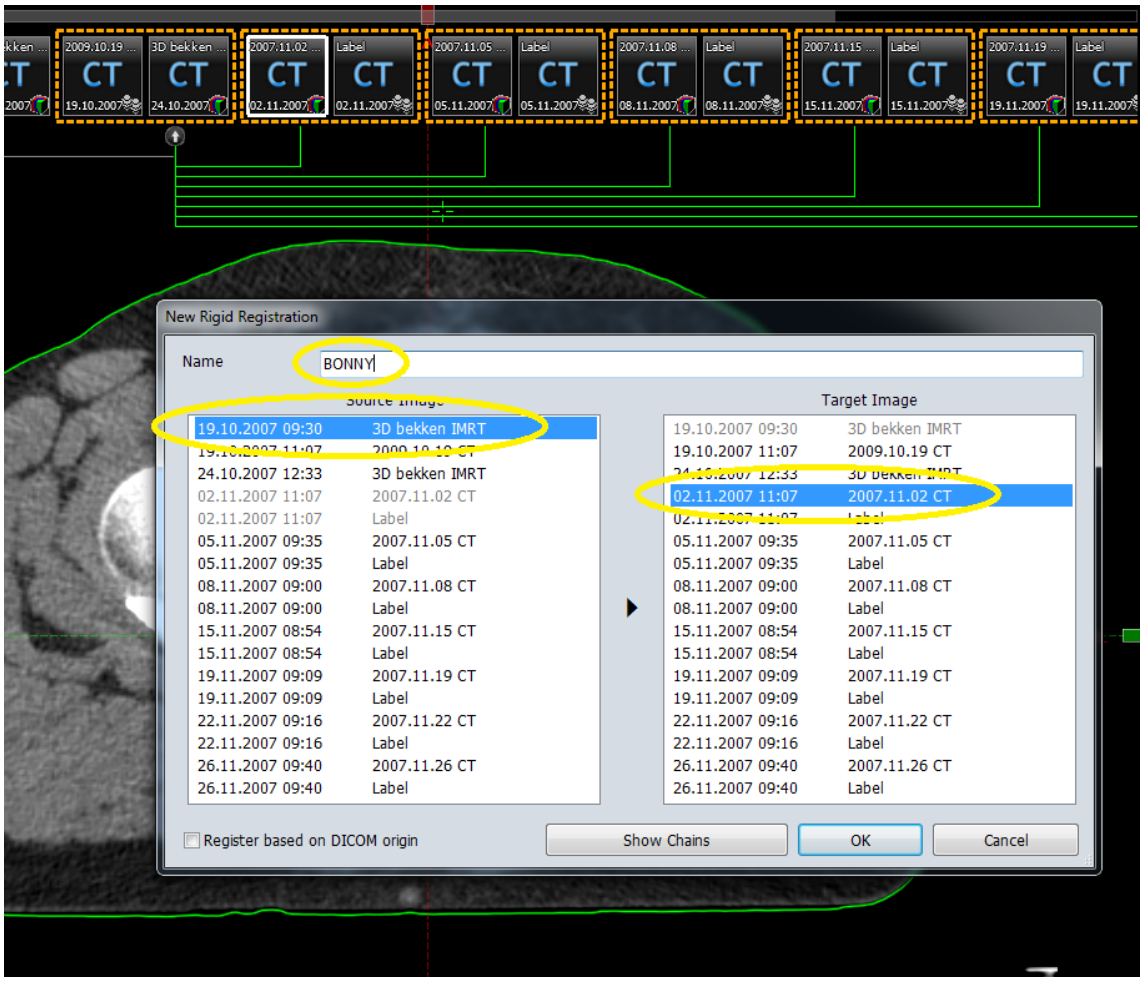

f) After clicking OK, a box (registration box) appears that can be adjusted to cover all the areas of interest. A volume of interest was placed around the pelvic bones including the prostate to restrict the registration area. Also a dialogue box pops up that you can turn off rotation as well as choose intensity range.

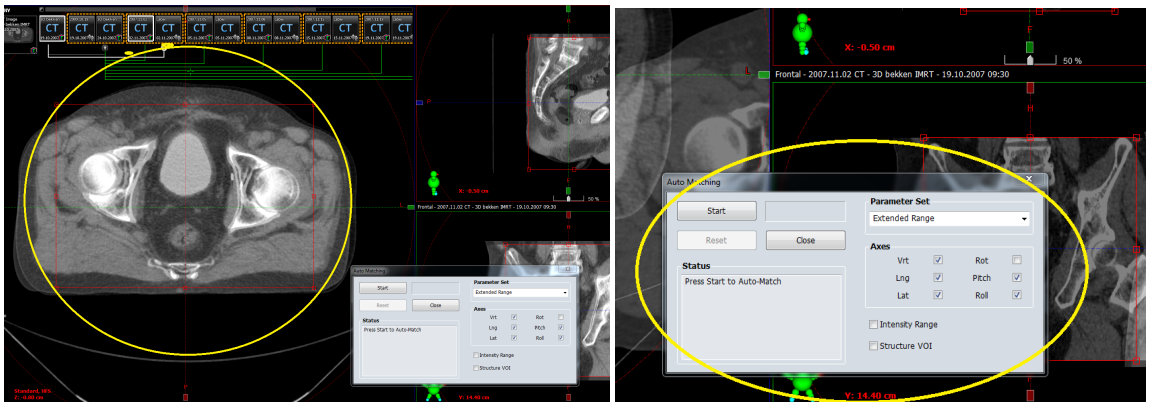

g) In this study, intensity of bones was being used as the registration was based on BA, so the box for bones was checked.

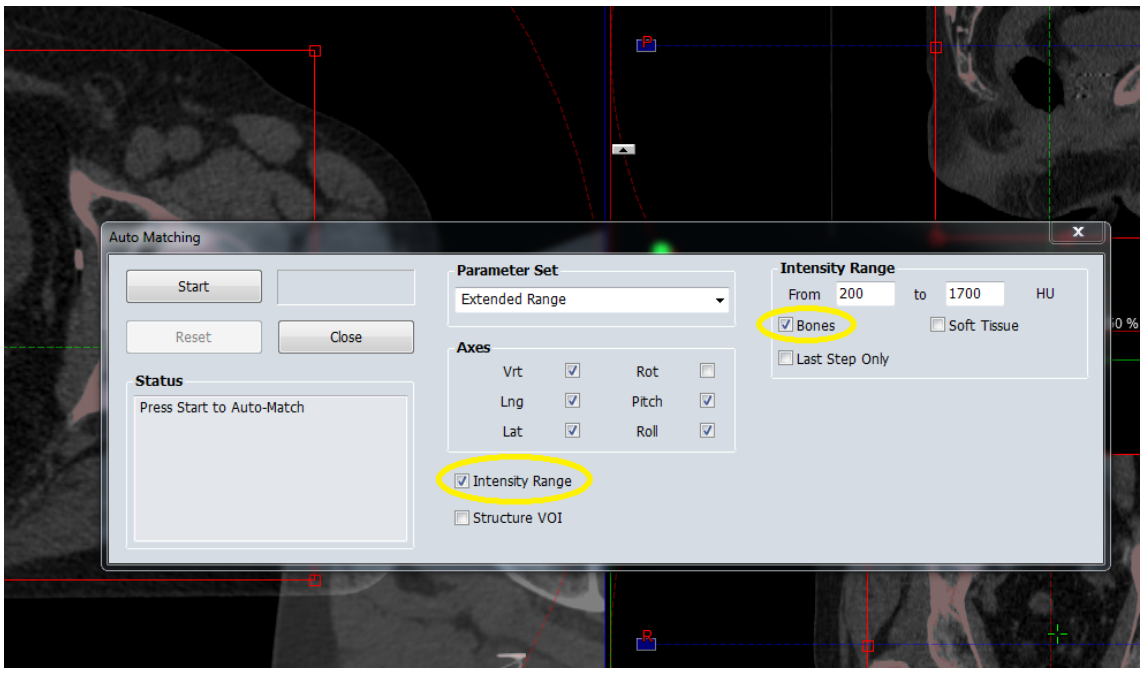

h) After the box was adjusted to cover all the bones in the area of interest, start the registration by clicking on start.

i) When the registration is finished then you click close.

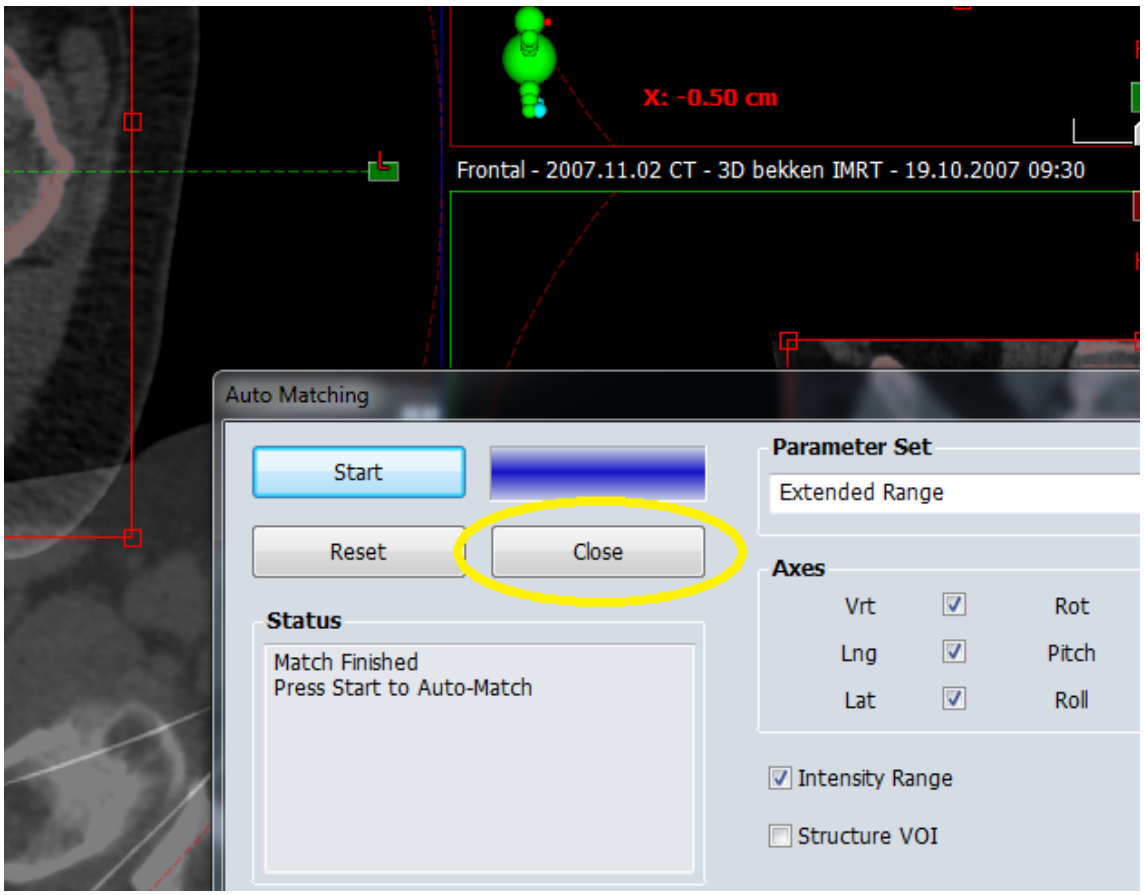

j) If it is satisfactory, the registration is done otherwise adjust the box to cover the bones again as you scroll from top to bottom and start the auto match again.

APPENDIX B
Procedure for creating structures in conservative treatment planning

a) When you login to the Eclipse TPS; you go to contouring, choose the patient you want to create the different structures, choose "insert" then new structure and finally click ok or right click on any existing structure and choose create structure. This will give you an option to name the structure, choose the type of structure and change the colour of the structure.

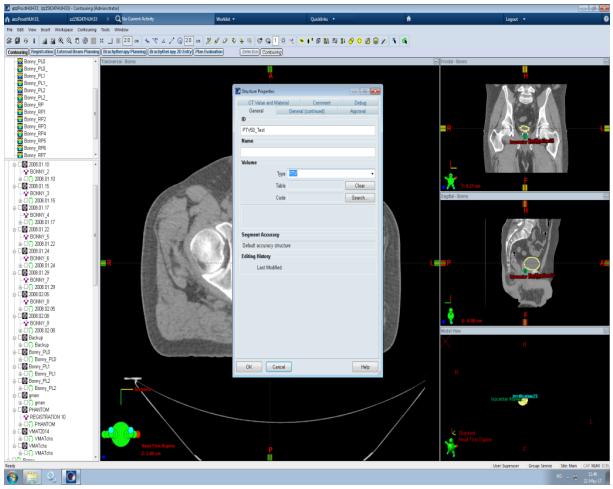

b) Highlight the structure newly created empty structure and click create margin. This will give you an option to choose the structure from which the structure will have its margin around or within as well as choose the margin for the different directions and you click okay. The structure will have been created.

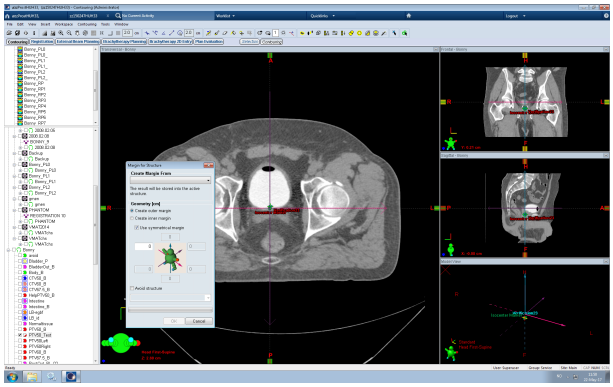

c) To create PTV50, use CTV50 plus 5 mm isotropical margin, then create PTV50Left and PTV50Right by deleting the part which should not be included. Use Boolean to include PTV6, using PTV50left Or PTV60.

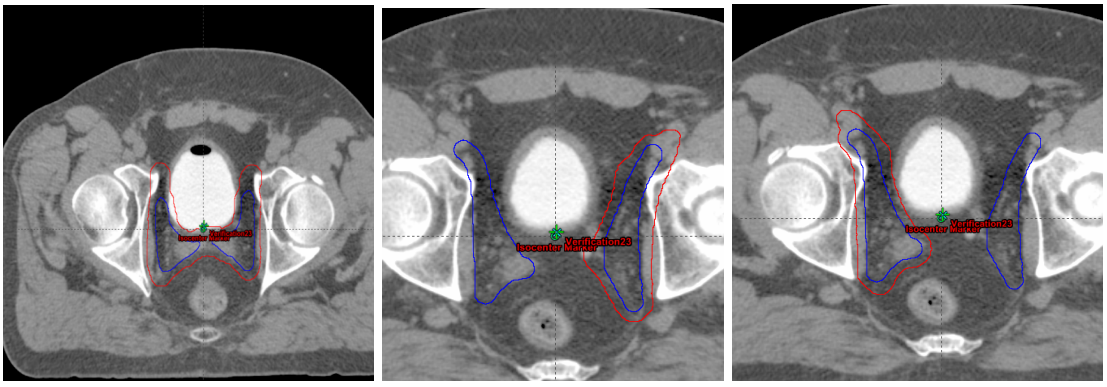

d) To create PTV60, use CTV60 plus 5 mm margin in the Left-Right direction and 10 mm otherwise.

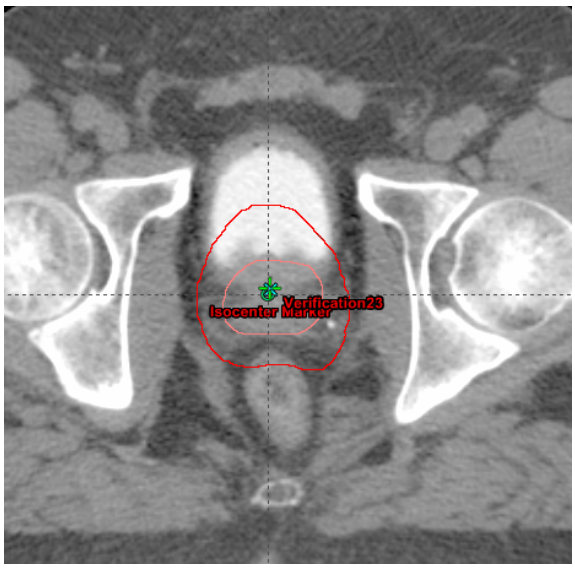

e) To create PTV67.5, use CTV67.5 plus 3mm margin in the Left-Right direction and 10mm otherwise.

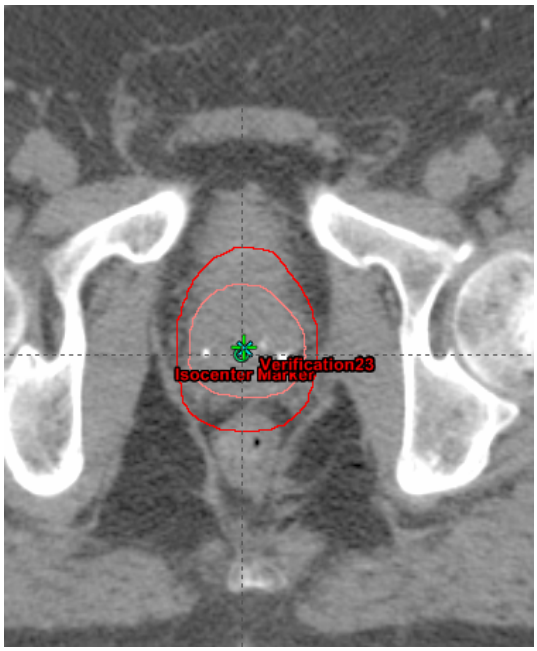

f) Create help volume, helpPTV50 from PTV50, crop towards PTV60 with 5 mm margin.

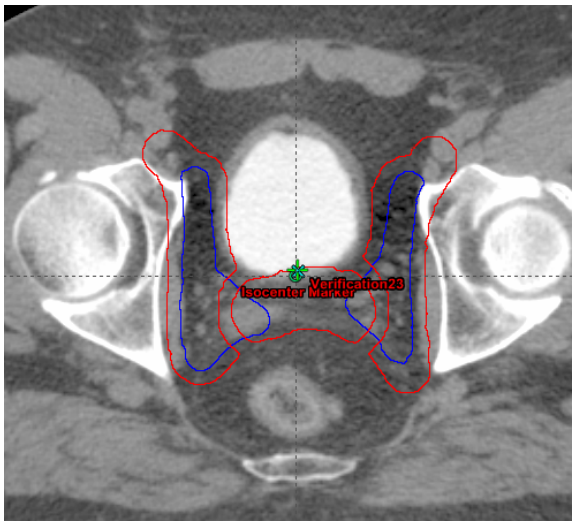

g) Create normal tissue (pink), 4 cm margin (1 cm cranial/caudal) around PTV50. Post processing: Extraction, keep 1 largest and connect 4 cm. Crop normal tissue towards PTV50 with 5 mm margin, crop towards PTV60 with 5mm margin and crop towards body with 1-1.5 cm margin. NB: Do connection before cropping.

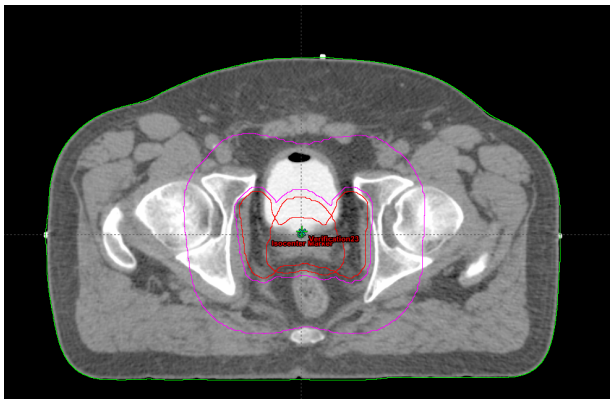

h) Create under67.5 around PTV67.5 with a margin of 2cm. Crop 5 mm towards PTV67.5.

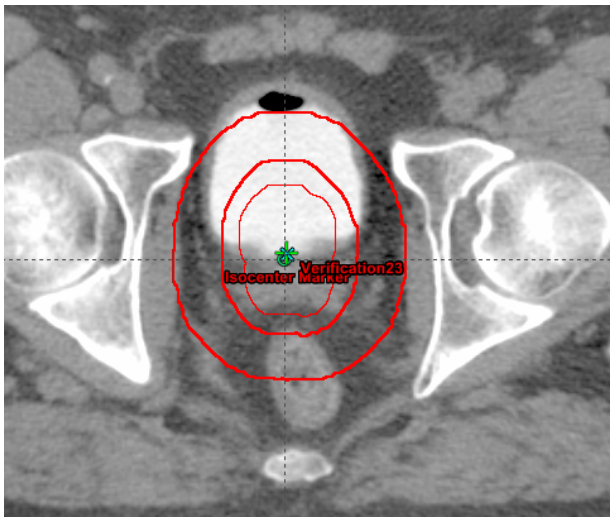

i) Create out volumes for BladderOut (pink), and crop 5mm towards PTV60 and PTV50.

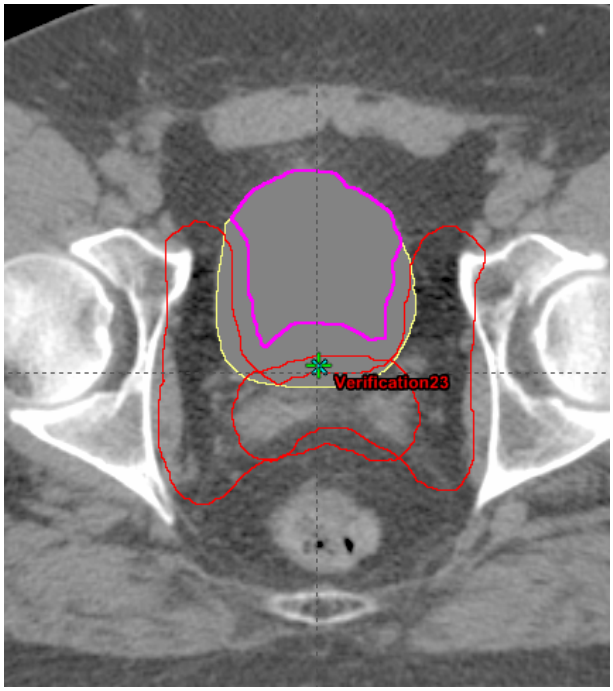

j) Create IntestineOut and crop 5 mm towards PTV50.

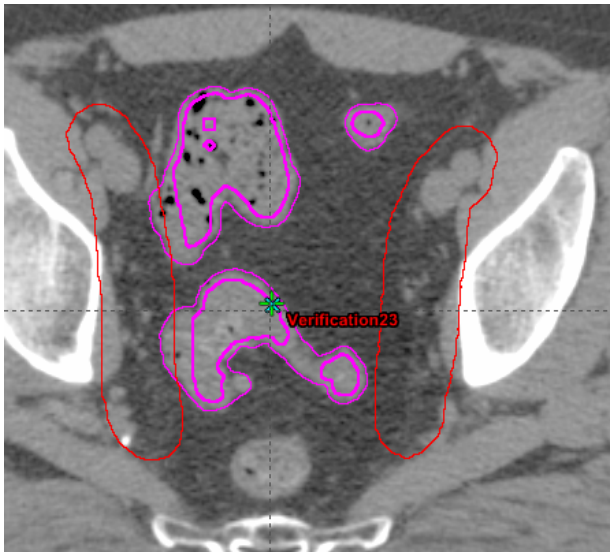

k) Create RectumOut (bold pink) and Crop 5 mm towards PTV60.

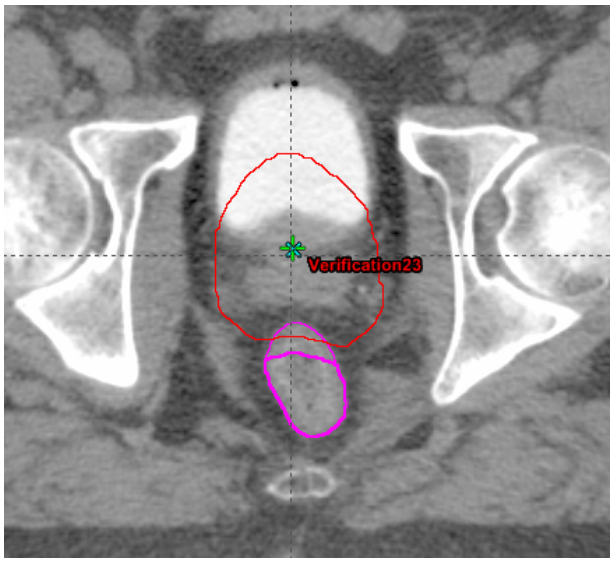

APPENDIX C
Procedure for creating structures in plan library treatment planning

a) When you login to the Eclipse TPS; you go to contouring, choose the patient you want to create the different structures, choose "insert" then new structure and finally click ok or right click on any existing structure and choose create structure. This will give you an option to name the structure, choose the type of structure and change the colour of the structure.
b) Highlight the structure newly created empty structure and click create margin. This will give you an option to choose the structure from which the structure will have its margin around or within as well as choose the margin for the different directions and you click okay. The structure will have been created.
c) Create PTV50; use CTV50 plus 5 mm isotropical margin.

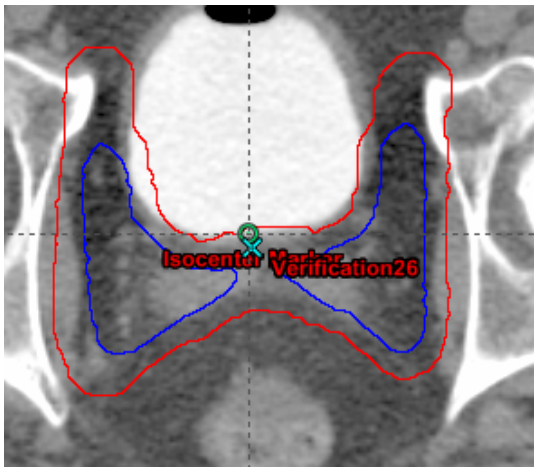

d) Create PTV50Left and PTV50Right by deleting the part which should not be included. Use Boolean to include PTV60, using PTV50left Or PTV60 for left and "PTV50Right or PTV60" for right.

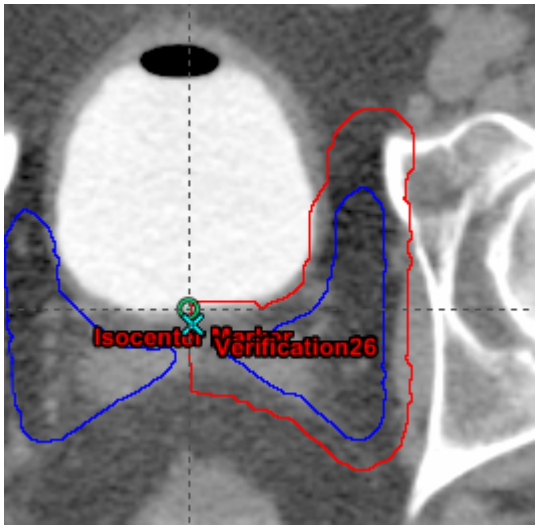

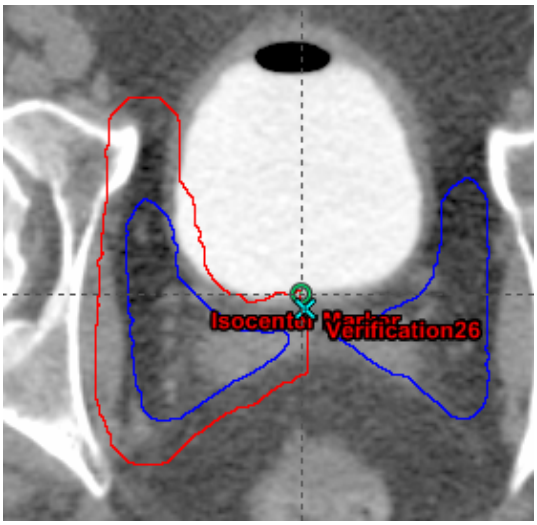

e) Use Boolean to include PTV60, using PTV50left or PTV60 for the PTV50left and PTV50Right or PTV60 for

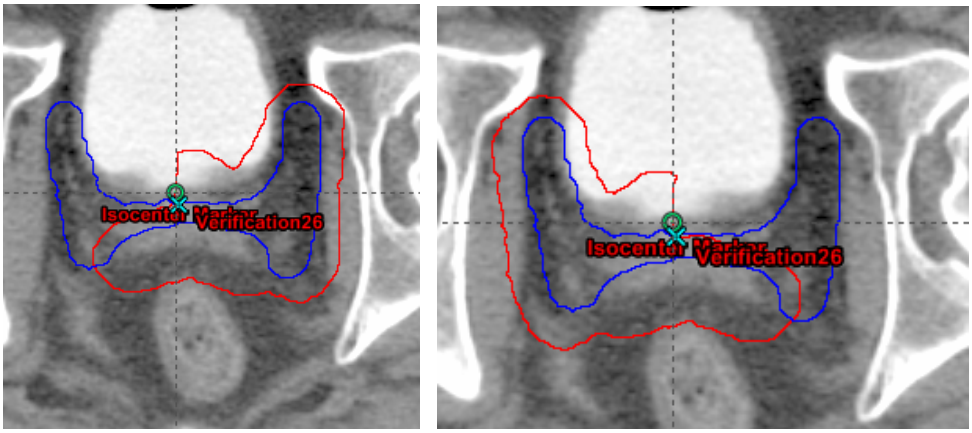

f) Create PTV60; use CTV60 plus a 5 mm isotropic margin.

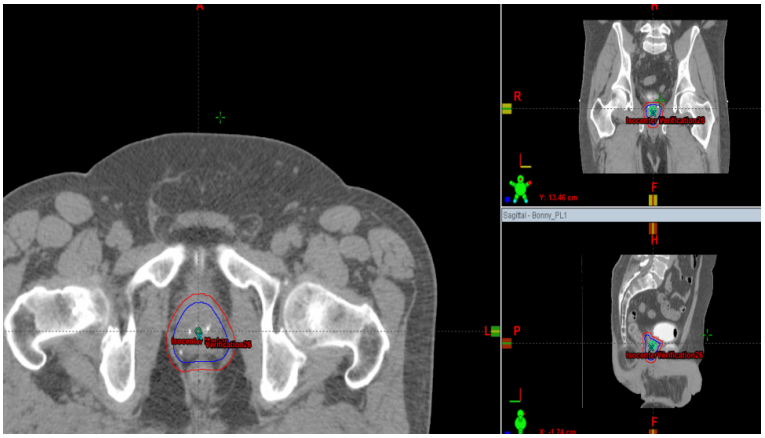

g) Create PTV67.5; use CTV67.5 plus a 5mm isotropic margin.

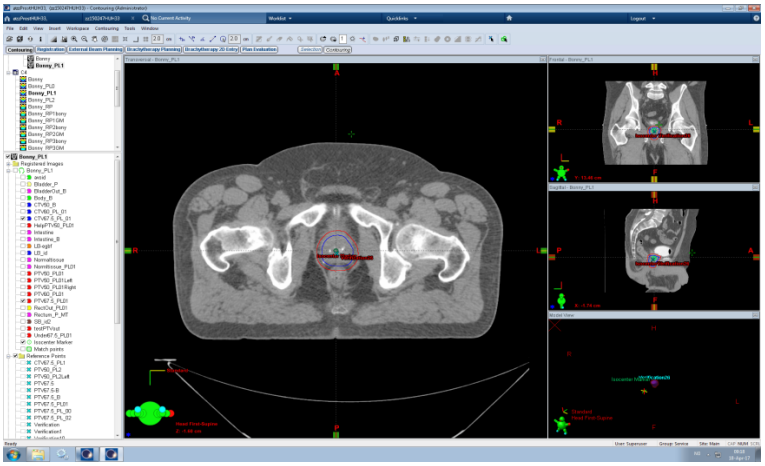

h) Create help volumes for helpPTV50 from PTV50, crop towards PTV60 with 5 mm margin.

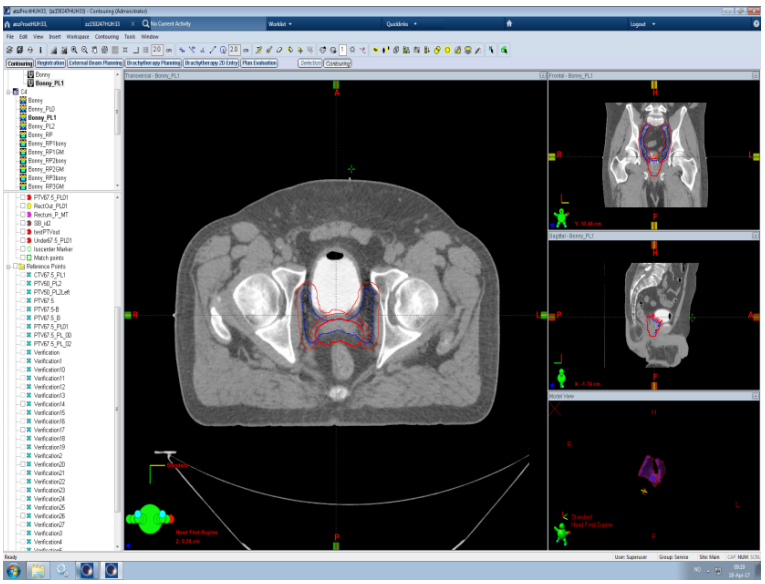

i) Create normal tissue, 4 cm margin (1 cm cranial-caudal) around PTV50. Post processing: Extraction, keep 1 largest, connect 4 cm. Crop normal tissue towards PTV50 with 5 mm margin, crop towards PTV60 with 5mm margin and crop towards Body with 1-1.5 cm margin. NB: connection before crop.

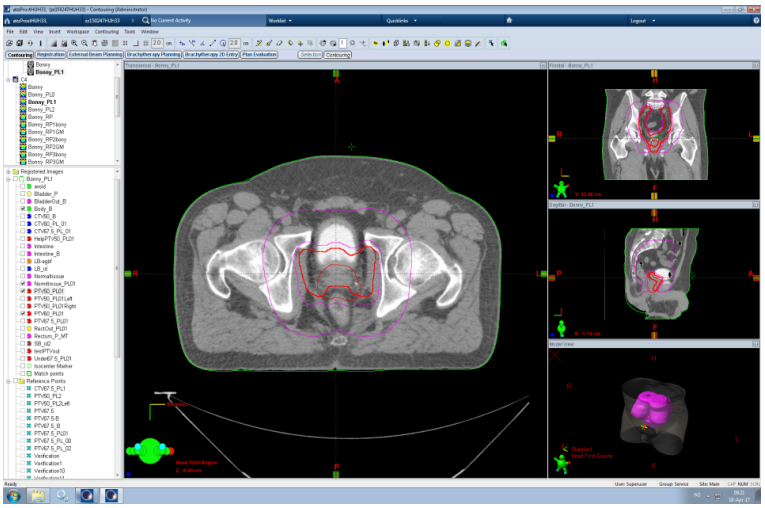

j) Create under67.5 around PTV67.5 with a margin of 2cm. Crop 5 mm towards PTV67.5.

k) Create out volumes for BladderOut and crop 5mm towards PTV60 and PTV50.

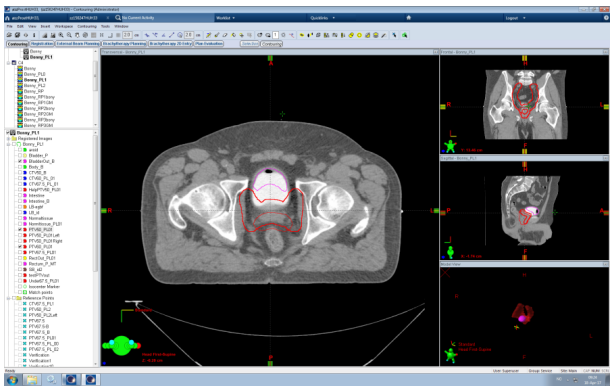

l) Create out volumes of RectumOut, Crop 5 mm towards PTV60.

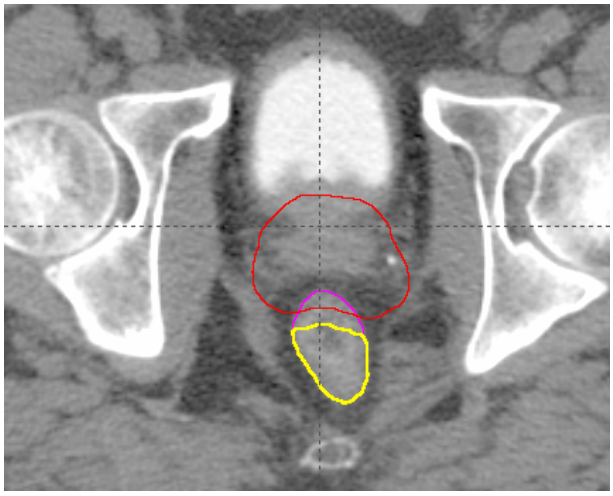

APPENDIX D
Procedure for plan selection

a) Create a new course and copy all the plans to that new course.
b) Create a verification plan for each of the positions of the prostate and remember to use "current structure".
c) Use the registration data and choose the most appropriate plan that seems to be the right directional shift (compared to AP=5, CC=4.6) for each rCT.
d) Drag and drop the chosen plan.
e) Press CTRL and right click on the rCT you want to choose the plan library for.
f) Inspect how the CTV60 and CTV67.5 for the rCT fit with the PTV60 and PTV67.5 of the pCT.
g) Copy the verification plan for the chosen plan that fitted well to its corresponding rCT and re-calculate the dose.
To create a verification plan; select the plan and go to;
1. Planning:

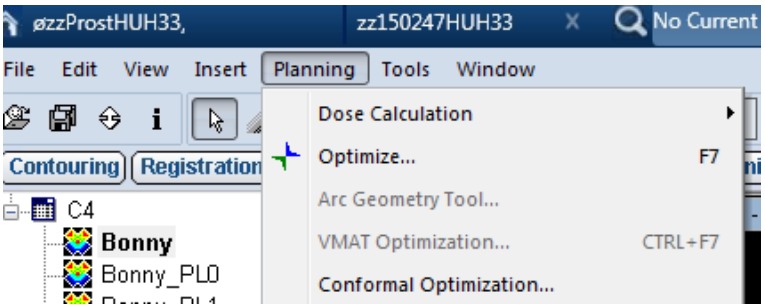

2. Create verification plan:

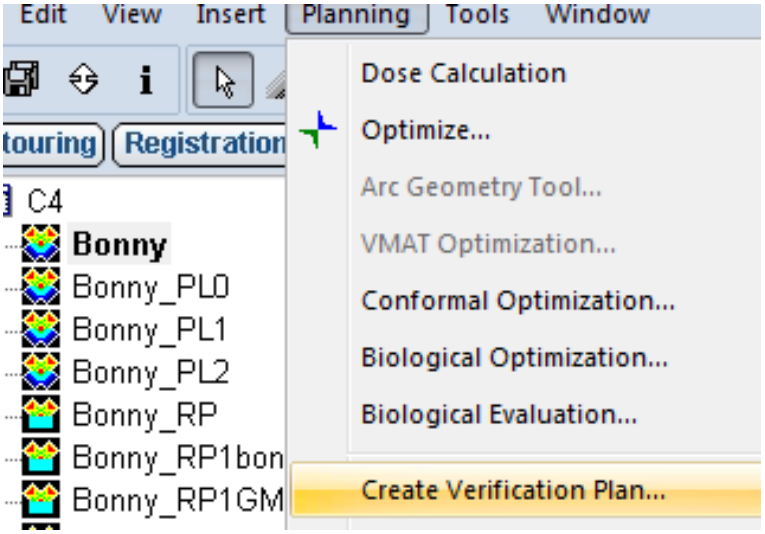

3. Select the location of the plan, in this case C4PL:

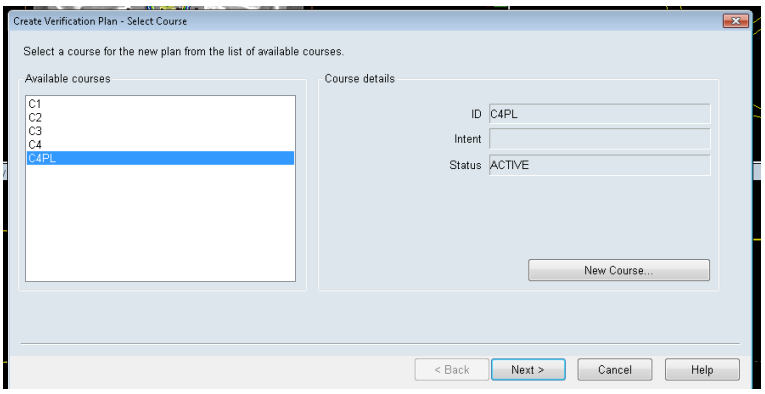

4. Select "use current" followed by next:

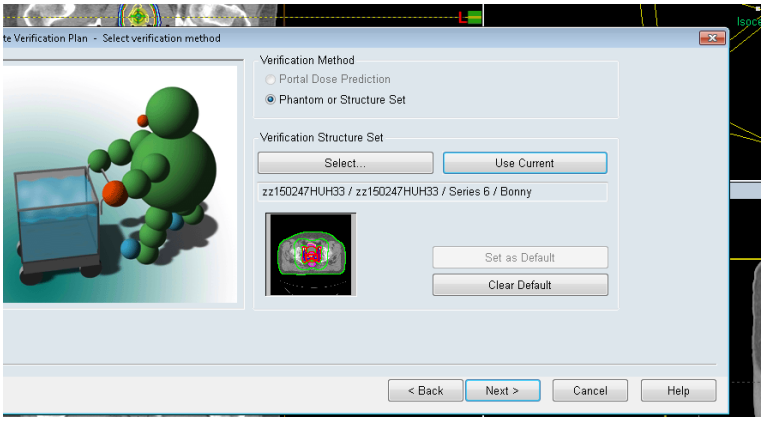

5. When done with creating the verification plan, copy and paste in each registration of the rCT and calculate the monitor units.
To create verification plans based on GM and bony anatomy registrations:
1. Define user origin inside prostate. This is done by dragging the mark into the prostate.
2. Create user origin structure in user origin. This is done by going to create new structure and use the brush to fit it onto the mark.
3. Define user origin in the same position on the GM registration rCT. This is done by pressing CTRL and right clicking the appropriate rCT; then drag the lines to cross in the mid-point.
4. Create GM verification plan (Under planning). Remember to select structure for each GM registration.
5. Do dose recalculation.
6. Name ID- in our case Bonny_RPXGM.
7. Then go to registration and delete the registration based on GM.
8. Note the isocentre of the robust plan.
9. Copy Bonny_RP to BonnyX registration image.
10. Create verification plan, change isocentre, change coordinates and scale the dose.
11. Create verification plan.
12. Rescale dose to 67.5 by changing fractions to 25.
13. Create Bonny_RPXbony plan.